Heat capacity, configurational heat capacity and fragility of hydrous magmas

D. Di Genova, Claudia Romano, Daniele Giordano, Marina Alletti

Heat capacity, configurational heat capacity and fragility of hydrous magmas

D. Di Genova[1*], C. Romano[1], D. Giordano[3], M. Alletti[2]

[1]Dipartimento di Scienze, Università degli Studi Roma Tre, L.go San Leonardo Murialdo 1, 8 00146 Rome, Italy

[2] Institut des Sciences de la Terre d'Orléans, INSU/CNRS-Université d'Orléans, Université François Rabelais de Tours, UMR 6133, 1A, rude de la Férollerie, 45071 Orléans Cedex 02, France

[3]Dipartimento di Scienze della Terra, Università degli Studi di Torino, Via Valperga Caluso, 35, 10125 Torino, Italy

*Corresponding author details phone: +39 06 57338061 fax: +39 06 57338201

e-mail: danilo.digenova@uniroma3.it

Abstract

The glassy and liquid heat capacities of four series of dry and hydrous natural glasses and magmas as a function of temperature and water content (up to 19.9 mol%) were investigated using differential scanning calorimetry (DSC). The analyzed compositions are trachybasalt, latite, trachyte and pantellerite. The results of this study indicate that the measured heat capacity of glasses (Cp_g) is a linear function of composition and is well reproduced by the empirical model of Richet (1987). For the investigated glasses, the partial molar heat capacity of water can be considered as independent of composition, in agreement with Bouhifd et al. (2006). For hydrous liquids, the heat capacity (Cp_{liq}) decreases non linearly with increasing water content. Previously published models, combined with the partial molar heat capacity of water from literature, are not able to reproduce our experimental data in a satisfactory way. We estimate the partial molar heat capacity of water (Cp_{H2O}) in hydrous magma over a broad compositional range. The proposed value is 41.38 J/mol K. As water dissociates in the silicate melt as hydroxyl groups and molecular species, we also calculated the partial molar heat capacity for each water species (Cp_{H2Omol}; Cp_{OH-}) and composition. The partial molar Cp_{H2Omol} and Cp_{OH}^{-} can be considered dependent of composition varying with the overall content of network modifier oxides (SM parameter, Giordano and Dingwell, 2003a). Water strongly affects the configurational heat capacity at the glass transition temperature [Cp^{conf} (Tg)]. An increases of Cp^{conf} (Tg) with water content was measured for the polymerized liquids (trachyte and pantellerite), while an opposite behavior could be observed for the most depolymerized liquids (trachybasalt and latite). Structural and rheological implications of this behavior are discussed in light of the presented results.

Keywords: Heat capacity, configurational heat capacity, fragility, water, magma

1. Introduction

Physical and thermodynamic properties of silicate melts are key factors governing petrological and volcanic processes such as melt generation, transport, emplacement, crystallization, degassing and eruptive style (e.g., Lange and Carmichael, 1990; Dingwell et al., 1996; Ochs and Lange, 1999; Papale et al., 1999; Snyder, 2000; Spera, 2000; Dingwell, 2006). Several studies performed on silicate glasses and liquids have demonstrated that anhydrous chemical composition and water, the most abundant volatile in magmatic systems, strongly affect the structure (e.g., Stolper, 1982a,b; Mysen et al., 1982; Mysen, 1997; Xue X., 2009; Mercier et al., 2009), the physical properties (viscosity, diffusivity, density, heat capacities; Persikov et al., 1990; Ochs and Lange, 1999; Whittington et al., 2000, 2009; Romano et al., 2001; Bouhifd et al., 2006; Vetere et al., 2007; Behrens and Zhang, 2009; Giordano et al., 2009; Fanara et al., 2012; Di Genova et al., 2013), the phase relationships and crystallization behavior of magmas (Fenn, 1977; Muncill and Lasaga, 1988; Davis et al., 1997; Vona and Romano, 2013). The isobaric heat capacity (Cp) is a thermodynamic property related to variations in the internal energy in a system and to structural changes of the silicate framework in response to temperature variations. Understanding how Cp varies with composition and water content is crucial in order to construct thermal models of petrological and volcanic processes, such as phase equilibra calculations, theoretical investigation of physical properties of liquids and water exsolution during ascent-driven degassing (e.g., Burnham and Davis, 1974; Ghiorso and Sack, 1995; Papale, 1997; Moretti and Papale, 2004; Papale et ., 2006; Richet et al., 2006; James et al., 2009; Whittington et al., 2009; Iacono-Marziano et al., 2012).

In addition, knowledge of the heat capacity of liquids helps to quantify the configurational entropy of magmas through the Adam and Gibbs (1965) theory of relaxation processes (Richet, 1984). It has been observed that the partial molar heat capacity of a single oxide ($Cp_{,i}$) in a glass is independent of composition (Stebbins et al., 1984; Richet, 1987). The three-term Maier Kelley equation, based

on the additive models of calculation from oxide components, well reproduces the variation of heat capacity of glasses (Cp_g) with temperature (Richet, 1987; Bouhifd et al., 2006). Heat capacity measurements on liquids performed on a simple Al-free silicate system have shown that Cp can be considered a linear function of oxide concentration, resulting in predictive models that assume ideal mixing of oxide components, each of with a partial molar heat capacity (e.g., Stebbins et al., 1984; Richet and Bottinga, 1985; Lange and Navrotsky, 1992). However, simple additive models fail to reproduce the heat capacities of aluminosilicate liquids, for which, no linear variations of heat capacity with compositions have been observed. This behavior has been generally attributed to the non-ideal mixing of oxide components to represent the heat capacity of silicate melts (Richet and Bottinga, 1985; Stebbins et al., 1984; Richet and Neuville, 1992; Bouhifd et al., 1998; 2012). In addition to that, despite the recent advances and large amount of data produced in literature over the last few decades, there is no unanimous consensus over the variation of heat capacity for hydrous natural glasses and liquids.

Burnham and Davis (1974) and Clemens and Navrotsky (1987) determined a partial molar heat capacitiy for water in hydrous melt of 80 J/mol K by performing calorimetric measurements and thermodynamic calculations on the albite-water system. Furthermore, Clemens and Navrotsky (1987) showed that this value is close to that predicted for pure water at P and T, suggesting that the partial molar heat capacity of water has little dependence on composition. About twenty years later, Bouhifd et al. (2006) measured the heat capacity of water for hydrated iron-free polymerized aluminosilicate glasses and liquids of albitic, phonolitic, trachytic and leucogranitic compositions. They argued, based on the Richet (1987) model, that water has a small effect on the heat capacities of silicate glasses, showing that the partial molar heat capacity of water can be considered as independent of glass composition and varies as a function of temperature as follows: $Cp_{H2O} = -122.319 + 341.631 * 10^{-3} T(K) + 63.4426 * 105 * T^{-2}$ (J/mol K). For liquids, Bouhifd et al. (2006) reported a value of partial molar heat capacity of water (Cp_{H2O} = 85 J/mol K) independent of liquid

composition and water content for the studied compositions. Recently, Bouhifd et al. (2012) presented new data for more depolymerized iron-free analogs (liquid and glasses) of tephritic and foiditic composition. The partial molar heat capacity of water reported in Bouhifd et al. (2006) for polymerized silicate glasses is similar to the values observed for these depolymerized compositions, suggesting, that the partial molar heat capacity of water in glasses is independent of composition. However, for depolymerized liquids, the authors reported a partial molar heat capacity of water of 237 J/mol K, suggesting a dependency of the heat capacity of water upon the degree of polymerization of the melts.

In order to address the effect of water on the heat capacity of silicate glasses and melts, we have investigated the Cp_g and Cp_{liq} of dry and hydrous remelted volcanic materials. We selected four natural compositions: trachybasalt from Mt. Etna (ETN, Giordano and Dingwell 2003a; Vona et al., 2011); latite from Fondo Riccio – Phlegrean fields (FR, Giordano et al., 2006; Misiti et al., 2011); trachyte from Agnano Monte Spina – Phlegrean fields (AMS-B1, Romano et al., 2003) and pantellerite from Pantelleria Island (PS, Di Genova et al., 2013). The compositions selected allowed us to fully explore the wide chemical variation characterizing natural magmas, and enabled us to address in detail the effect of specific chemical parameters on the internal energy of the liquids. At the same time, as the rheological behavior of those liquids is well characterized in the literature, a comparison between viscosity and configurational heat capacity allowed us to calculate and discuss the configuration entropy and fragility of these liquids and their variation as a function of water content in the magma.

2. Experimental methods

2.1. Synthesis of hydrous samples

The starting glassy dry materials were obtained by direct fusion of natural pantellerite (PS), trachyte (AMS-B1), latite (FR) and trachybasalt (ETN) magmas. The natural materials were melted

in a large thin-walled Pt crucible in a Nabertherm $MoSi_2$ box furnace at T = 1400-1600 °C for a few hours. The melts were then quenched in air, and samples were removed from the crucibles. Chips of glass were loaded into a $Pt_{80}Rh_{20}$ cylindrical crucible and remelted in a box furnace heated by $MoSi_2$ elements (Theta ®) and stirred using a Paar Rheolab QC ® rheometer (EVPLab Rome Tre University). Stirring allowed complete homogenization and removal of bubbles from the samples. Subsequently, the melt was cooled in air and the glasses obtained were used for the chemical characterization of dry material. The major element composition of the glasses was determined at the CNR – *Istituto di Geologia Ambientale e Geoingegneria* in Rome, using a Cameca SX50 electron microprobe, with 5 WDS spectrometers and EDS Link eXL system, under analytical conditions of 15 kV accelerating voltage, 15 nA beam current and 10 μm beam diameter to reduce K and Na volatilization. Chemical analyses are reported in Table 1.

In order to synthesize hydrous samples, the glassy dry materials were powdered and loaded together with known amounts of distilled water into platinum capsules with 2.9 mm outer diameter, 2.5 mm inner diameter and 20 mm height. A rapid-quench-internally-heated pressure vessel (IHPV, CNRS/INSU-Universitè d'Orleans) was used to synthesize water-bearing samples, containing up to 19.9 mol% H_2O, at P= 4 kbar, T=1200-1400°C (Tab. 2). To check that water did not leak from the capsules, the capsules were weighed before and after being placed in an oven for at least one hour and no weight difference was observed. Homogeneity and absolute water content of the hydrated samples were determined by Karl-Fischer Titration (Hannover University), following the method described by Behrens et al. (1996) and Nowak and Behrens (1997). To correct for unextracted water after KFT, a quantity of 0.10 wt% was added to the measured values (Behrens and Stuke, 2003) for AMS-B1 and PS samples. In order to check water homogeneity distribution and possible loss of water during the calorimetric and viscosity measurements, Fourier transform infrared (FTIR) spectroscopy was performed before and after each experiment. 4500 cm^{-1} (OH^- groups) and 5200 cm^{-1} (H_2O molecules) peak heights of the near-infrared (NIR) absorption bands were used to

analyze the water content of the samples using the Lambert–Beer law (Stolper, 1982a). Infrared absorption spectra were collected on doubly polished glass chips with thickness ranging from 260–350 µm. The water content of the nominally dry starting glasses was determined by measuring the peak height of the mid-infrared (MIR) absorption band at 3550 cm^{-1}. FTIR spectra were collected at the Laboratory of Infrared Spectroscopy, Department of Science (University Roma Tre), using a NicPlan IR-microscope equipped with a liquid nitrogen-cooled MCT detector. The nominal resolution was 4 cm^{-1} and 128 scans were averaged for each sample and for the background. Simple linear baselines were fitted to both NIR peaks (TT baseline according to Ohlhorst et al., 2001). Molar absorption coefficients used for each composition are reported in Table 2. Uncertainty of the results is about 2% based on the reproducibility of measurements and on the error associated with the background subtraction procedure. Archimedean buoyancy was performed to measure densities of dry and hydrous glasses. Thickness was measured with a digital micrometer with an uncertainty of ± 5µm. Results of the water determinations are reported in Table 2, together with synthesis conditions.

2.2. Calorimetry

Calorimetric measurements were performed by Differential Scanning Calorimeter technique (Netzsch ® DSC 404 Pegasus, EVPLab Rome Tre University). Prior to analysis of the samples, temperature and sensitivity calibration was performed using melting temperatures of standard materials (In, Sn, Bi, Zn, Al, Ag and Au) up to 1000°C. Subsequently, a baseline measurement was taken where two empty Pt/Rh crucibles were loaded into the DSC and then the DSC was calibrated against the Cp of a single sapphire crystal (Robie et al.,1979).

Doubly polished glass samples 30 to 60 mg of weight were placed in Pt crucibles under a constant Argon flow rate (20 lt/min). Each sample was heated at 1 K/min heating rate from room temperature to 323 K and kept at this temperature for approximately one hour in order to achieve

DSC signal equilibrium. Subsequently, in order to attain the structural relaxation of the high pressure liquids, temperature was raised with a heating step of 20 K/min from T = 323 K up to maximum 50 K above estimated glass transition temperature (Tg) of the sample. Cooling rate after the experiment matched the heating rate (20 K/min).

Measurements of Tg and Cp were performed in 3 subsequent thermal treatments where the heating rates always matched the previous cooling rates (20 – 10 – 5 K/min). The heat capacity versus temperature paths did not show any evidence of water exsolution, crystallization or weight loss during the experiments. Post run optical analysis performed after each experiment confirmed the absence of thermal alteration of the samples.

3. Results

3.1. Heat capacity and glass transition temperatures (Tg)

The heat capacities and the glass transition temperatures (Tg) of the silicate liquids investigated in this study are reported in Tab. 3 and shown in Fig. 1 (a, b, c, d) as a function of composition, temperature and water content. The heat capacity (Cp) measurements were carried out on nominally anhydrous samples and hydrous samples containing up to 19.9 mol% H_2O in the temperature range of 574 – 1002 K.

Except for liquids of some specific composition as titanosilicates and borosilicates (e.g., Richet and Bottinga, 1986; Lange and Navrotsky, 1993; Richet et al., 1997), it is generally observed that the heat capacity of silicate liquids (Cp_{liq}) is constant with temperature, and this allows for extrapolation in a large T interval (e.g., Richet and Bottinga, 1986; Lange and Navrotsky, 1993; Bouhifd et al., 2006). In the temperature range investigated above the Tgs, no variation of was observed, in agreement with literature studies.

Trachybasalt liquid from Etna (ETN) shows the highest dry liquid heat capacity Cp_{liq} = 96.6 J mol^{-1} K^{-1}, followed by latitic sample from Fondo Riccio (FR , Phlegrean Fields) with a Cp_{liq} = 94.8 J mol^{-1} K^{-1}, pantellerite from Pantelleria (PS) with a Cp_{liq} = 91.6 J mol^{-1} K^{-1} and trachytic liquid from Agnano Monte Spina, Phlegrean Fields (AMS-B1) with a Cp_{liq} = 90.5 J mol^{-1} K^{-1}.

As can be seen from the Cp curves in Fig. 1, the liquid heat capacity of the silicate melts (Cp_{liq}) decreases with increasing water content for each composition. The variations of Cp_{liq} as a function of water content is shown in Fig. 2. Upon initial dissolution of water (up to 5 mol% H_2O), a small decrease of heat capacity can be observed for all liquids. As additional amounts of H_2O are introduced in the melts, the Cp_{liq} seems to decrease more strongly converging to similar values for all compositions. From the heat capacity curves we derived glass transition temperatures, defined as the temperature at which the response of a magma changes from an equilibrium to a solid-like, glassy response.

In order to characterize the cooling/heating rate dependence of the calorimetric glass transition temperatures (Tg), measurements were performed at heating/cooling rates of 5, 10, 20 K/min following the method described by Giordano et al., (2008). The values of the measured glass transition temperature, as collected at the peak (Tg_{peak}), onset (Tg_{onset}) and stable liquid (Tg_{liquid}) position of the heat capacity curves (Fig. 3), are listed in Table 3. Fig. 4 shows the strong positive correlation between glass transition temperatures determined at the onset, peak and liquid, as also shown by Giordano et al., (2005; 2008). The values of the measured glass transition temperatures, as collected at the peak and at the onset are reported in Fig. 5 for each specific composition, H_2O content and thermal treatment. Liquid Tgs are affected by larger error compared to the onset and peak measurements and for this reason they have not been considered in the following discussion. Peak and onset Tgs correlate very well showing similar trends of variation as a function of anhydrous composition, H_2O content and thermal treatment. In general, peak Tgs show consistently higher values (approximately 50 K) compared to onset Tgs. For each composition, higher Tg values

are attained for cooling/heating cycles performed with the highest rates. The effect of water on the Tgs can be better evaluated by direct comparison of all liquids in Fig. 6. In the figure, the value of Tg_{peak} is chosen for convenience, as the measurement of Tg_{peak} is associated with the lowest standard error, and cooling/heating rates of 20 K/min were considered. The pantellerite samples (PS) show the lowest measured value of Tg both for anhydrous and for hydrous conditions. For instance, the dry Tg_{peak} exhibited by the PS pantellerite (Tg = 875 K), measured at 20 K/min, is about 110 K lower than the Tg_{peak} shown by the AMS-B1 trachyte (987 K) and FR latite sample (985 K), while it is 80 K lower than the Tg of the ETN trachybasalt (Tg = 954 K) (Tab. 3).
Glass transition temperatures appear also to be strongly dependent on water content, decreasing as water content increases in the melt (Fig. 5 and 6). The decrease appears to be sharper at lower concentrations of H_2O. Among the liquids shown in Fig. 6, the PS pantellerite shows the lowest Tg over the entire range of water content investigated. (Tg_{peak} = 636 K at H_2O = 11.95 mol.%). The decrease in glass transition temperature due to the addition of water in the melt is most pronounced for the latitic sample (FR) that shows a decrease in Tg_{peak} of 294 K when 12.55 mol.% H_2O is added. AMS-B1 trachyte shows a decrease in Tg_{peak} of 275 K when 12.46 mol.% H_2O is added and ETN trachybasalt exhibits a decrease in Tg_{peak} of 224 K whit the introduction of 11.99 mol.% H_2O.

3.2 Water speciation

Water dissolved in the melt was measured both via Karl Fisher Titration and Fourier-Transform Infrared Spectroscopy. Spectroscopic measurements of water in the glasses quenched at 20K/min cooling rate after calorimetric measurements allowed for the determination of water species in the liquid frozen at Tg.

Table 2 illustrates the concentration of molecular water, hydroxyl groups and total water content expressed both in weight percent and in molar concentration (two oxygen basis), as determined by KFT analyses and FTIR. The molar absorption coefficients used for each investigated composition

are also reported in Tab. 2. The concentrations of molecular water and hydroxyl groups (expressed as mole % H_2O) as a function of increasing water content are also shown in Fig. 7. The concentrations of both species vary with composition with the molecular water increasing and the hydroxyl groups decreasing as the total water content in the melt increases. The concentration of molecular and hydroxyl groups is the same for water content of approximately 7 mole %. Similar abundances of OH^- and molecular H_2O species are largely shown in literature for a wide range of silicate composition (e.g., Stolper, 1982b; Behrens and Nowak, 2003; Lesne et al., 2011).

4. Discussion

4.1 Heat capacity of glasses

In this study we have reported calorimetric measurements for four series of natural dry and hydrous glasses and liquids of trachybasaltic (ETN); latitic (FR); trachytic (AMS-B1) and pantelleritic (PS) composition. In order to parameterize and compare our results with the Richet (1987) model, the measured heat capacity of silicates glasses (Cp_g, Tab. 3) have been reproduced via the Maier Kelley equations as follow:

$$Cp_g = a + bT + c/T^2 \quad (1)$$

where the a, b and c coefficients are reported in Tab. 4 together with the standard error. For the anhydrous glasses, calculated Cp using Eq. 1 is well predicted by the Richet (1987) model within 1.8%. Using the measured heat capacity of hydrous glasses, together with the Richet (1987) model for the anhydrous composition and considering a temperature dependence of Cpg_{H2O} as reported in Eq. 1, we derived the partial molar heat capacity of water in silicate glasses (Cpg_{H2O}, $R^2 = 0.92$) as following:

$$Cpg_{H2O} = 112.52 - 59.10\ 10^{-3}\ T - 77.20\ 10^{5}/T^{2} \quad (2)$$

The Cp of all hydrous glasses are reproduced within 4%, confirming that the partial molar heat capacity of water is independent of composition in silicate glasses over a broad range of degree of polymerization ($0 \leq NBO/T \leq 1.5$), in agreement with Bouhifd et al. (2006; 2012).

4.2 Heat capacity of anhydrous liquids and comparison with literature data

The measured heat capacities of anhydrous silicates liquids (Cp_{liq}, Tab. 3) have been compared with predicted values using the models of Stebbins et al. (1984), Lange and Navrotsky (1992) and Richet and Bottinga (1985) with the mean Cp of Al_2O_3 reported by Courtial and Richet (1993). In Tab. 5, the measured Cp_{liq} of the present study are compared with those predicted by these three models. We considered partitioning of Fe_{total} in equal amounts as FeO and Fe_2O_3 (in wt%; Giordano et al., 2006). We observe significant differences, expressed as $\Delta\% = [100*$ (Measured Cp − Calculated Cp) / Measured Cp], between the measured and calculated values. The measured anhydrous Cp_{liq} for the PS sample is reproduced within ±1.6% by all models. However, the Lange and Navrotsky (1992) and Stebbins et al. (1984) models strongly overestimate (by 7.7% and 4.8% respectively) the measured Cp_{liq} for AMS-B1, while the Richet and Bottinga (1985) model overestimates the measured Cp_{liq} for AMS-B1 by 3.5%. As far as the more depolymerized liquids are concerned, the Richet and Bottinga (1985) and Stebbins et al. (1984) models excellently reproduce (within 0.9%) the measured data for the ETN trachybasalt and for the FR latite (within 0.5% and 0.4% respectively). The Lange and Navrotsky (1992) model overestimates our data to a greater extent, with an error of 2.1% and 2.7% for ETN and FR, respectively. In summary, the Richet and Bottinga (1985) model seems to reproduce more closely our anhydrous dataset, showing the largest error (3.5%) for the AMS-B1. The Lange and Navrotsky (1992) and Stebbins et al.

(1984) models largely fail to reproduce the measured Cp for AMS-B1 and FR. A possible explanation for this resides in the high Al_2O_3 content of these liquids, much higher (12.29 and 11.68 mol% for AMS-B1 and FR respectively) compared to those for pantelleritic and trachybasaltic compositions (5.96 and 10.76 mol% respectively). Both Stebbins et al. (1984) and Lange and Navrotsky (1992) models are in fact ideal solution models in which the partial molar heat capacities of Al_2O_3 content is temperature independent. On the other hand, the model by Richet and Bottinga (1985), implemented by Courtial and Richet (1993), considers specific interactions between aluminum and alkali or other alkaline-earth elements which result in a temperature-dependent term for the Al_2O_3 Cp, more realistic for Al-rich compositions as AMS-B1 and FR liquids.

The anomalous heat capacity and its temperature dependence of Al_2O_3 also correlates with analogous complex volumetric and rheological behavior for this oxide. It is beyond the aim of this paper to address the issue of the structural role of the aluminum in melts, but certainly the reason of its complex behavior has to reside in the dual network-forming and network-modifier role of this element, in its capability to strongly interact and form complexes with alkalies and to assume different coordination states in different chemical environment (Mysen and Toplis, 2007).

4.3 Heat capacity of water in silicate liquids

The general effect of water is that of decreasing the heat capacity of silicate liquids (Fig. 1). In Fig. 2 the variations of Cp_{liq} as a function of mole percent of water is shown. The decrease of Cp as a function of water content for all compositions investigated here is not linear, being slight upon initial dissolution of water and much stronger as additional amounts of H_2O are introduced in the melts.

We compared our results for hydrous liquids with literature data. For the anhydrous silicate melt we considered the partial molar heat capacity of single oxides from the model of Richet and Bottinga (1985) which better reproduces our data. The partial molar heat capacity of water is poorly

constrained in literature. Bouhifd et al. (2006) published a value of 85 J/mol K for the heat capacity of water for polymerized melts (0 < NBO/T < 0.2), in agreement with the studies of Burnham and Davis (1974) and Clemens and Navrotsky (1987). Recently, a much greater value for the partial molar heat capacity of water of 237 J/mol K has been reported by the same authors (Bouhifd et al., 2012) for depolymerized melts of synthetic tephritic and foiditic composition (0.86 < NBO/T < 1.51).

In Table 5 we report calculations performed considering Bouhifd et al. (2006) value of 85 J/mol K for partial molar heat capacity of water for polymerized compositions and the Richet and Bottinga model (1985) for partial molar heat capacity of the other oxides. The parameterization is not able to reproduce our experimental data in a satisfactory way and the error between the measured and calculated values increases with increasing water content. For liquids with water contents of ~12 mol% (~3.5 wt% H_2O), the difference between measured and calculated values range between 3.7 to 8.5%. The calculated liquid heat capacities for our depolymerized melts considering the water partial molar heat capacity of Bouhifd et al. (2012) in depolymerized liquids (Cp_{H2O} = 237 J/mol K), and the Richet and Bottinga model (1985) for partial molar heat capacity of the other oxides, are reported in Table 6. As can been seen from Tab. 6, the calculated Cp extremely overestimate (up to 50%) our experimental data, suggesting again that the estimated values of partial molar heat capacities of water from literature are not able to reproduce our experimental results in any appreciable way. The causes of this lack of correlation could be diverse. It may be related to paucity of data at high water content (higher than 7 mol% of H_2O) or to the approximation resulting from linearly fitting the heat capacity versus water curves.

Moreover, the discrepancy could arise from compositional dependence terms for the heat capacity of water, as suggested by Bouhifd et al. (2012), or deviations for the ideal behavior of the solution assumed in the analytical approach, or the error deriving from the comparison of natural versus

synthetic composition. For instance, in our case, the presence of iron or other minor oxides could very well influence the calculation of the partial molar heat capacity of water.

Given the poor correlation of our data with existing literature, we decided to derive independently the heat capacity of water for each specific composition investigated in this study.

Treating the hydrous melt as a pseudo-binary mixture of an anhydrous silicate melt end-member and a pure water end-member one can write (Bouhifd et al., 2006):

$$Cp_{liq.} = X_{H2O}\, Cp_{H2O} + (1- X_{H2O})\, Cp_{liq.Anhydrous} \quad (3)$$

where X_{H2O} is the mole fraction of water, Cp_{H2O} is the partial molar heat capacity of water and $Cp_{liq.Anhydrous}$ is the heat capacity of anhydrous liquid.

Using the Eq. 3 and our experimental data, we derived partial molar Cp_{H2O} from the different liquids varying from 26.05 J/mol K (FR latite) to 56.64 J/mol K (PS pantellerite) with intermediate values for ETN (44.58 J/mol K) and AMS-B1 liquids (42.12 J/mol K). Although it is possible to discern a trend of decreasing partial molar Cp_{H2O} with NBO/T, the data are not robust enough to express this relationship in a quantitative way and additional studies on natural liquids are required to further investigate this issue. For this, we decided to neglect any compositional dependence and fit all data together. Using the Eq. 3 and our experimental data, we therefore derived 41.38 J/mol K as the partial molar heat capacity for water in natural silicate melts. In Tab. 5 we reported the calculated liquid heat capacity using the Eq. 3 together with the calculate partial molar heat capacity for water. Relative average error for the investigated data is in the order of 1.1 %. Therefore, using the anhydrous heat capacity reported in Tab. 5 for the investigated liquids with Eq. 3 and the derived partial molar heat capacity for water, it is easily possible calculated the liquid heat capacity variation with H_2O content.

Even though the approximation of a linear fitting of the data leads to excellent reproducibility of our results within the range of water content investigated in our study, contribution to the heat capacity of molecular (H_2O_{mol}) water versus hydroxyl species (OH^-) can also be extracted. In fact, when looking in detail at Fig. 2, the relationship between the measured Cp_{liq} and H_2O content is nonlinear. The heat capacity of liquids tends to remain constant from anhydrous condition to up to approximately 6 mol% H_2O, and then decreases as further water is dissolved into the melt. Similarly, it can also be observed (Fig. 7), that the relative concentration of water species in the melt varies in a non linear fashion. The relative abundance of H_2O_{mol} and OH^- molar species tends to be similar as the first 7 mol% H_2O is added to the melt, whereas a clear increase of H_2O_{mol} content, with respect to hydroxyl groups, is observed as increasing amount of water is dissolved (from 7 to 15 mol% H_2O). It should be noted that the measurements of the water speciation on glasses quenched from high temperature experiments do not represents isothermal values (e.g. Shen and Keppler, 1995; Romano et al., 1995; Behrens and Nowak, 2003), as the water species keep reacting during quenching and the reaction is actually frozen only at the glass transition temperature, which differs as a function of water content itself. However, as the calorimetric measurements are performed in the proximity of the glass transition temperature, and assuming the temperature does not affect considerably the anhydrous liquid heat capacities, comparison between the speciation curve and the calorimetric curve, although not isothermal, is still possible.

By assuming this, the nonlinear relationship between the Cp_{liq} and H_2O content (Fig. 2) can then be related to the non linear dependence of speciation on total water concentration, as also reported in Bouhifd et al. (2006; 2012). Taking into account the measured Cp_{liq}. shown in Tab. 3 and the measured water speciation data reported in Tab. 2, we have calculated the partial molar heat capacity for molecular water and OH^- ions, for each composition, modifying Eq. 3 as follow:

$$C_{pliq.} = X_{H2O\ mol.}\ Cp_{H2O\ mol.} + X_{OH-}\ Cp_{OH^-} + (1- X_{H2O})\ Cp_{liq.Anhydrous} \quad (4)$$

where X_{H2Omol} and X_{OH-} are the mole fraction of molecular water and OH^- ions respectively, Cp_{H2Omol} is the partial molar heat capacity of molecular water, Cp_{OH^-} is the partial molar heat capacity of OH^- ions and $Cp_{liq.Anhydrous}$ is the heat capacity of anhydrous liquid. X_{H2O} is as in Eq. 3. The calculated values of Cp_{H2Omol} and Cp_{OH^-} are reported in Tab. 7 and Fig. 8 as a function of the SM parameter from Giordano and Dingwell (2003a), which is calculated as the sum of the network modifier oxides (mole%), and is related to the degree of polymerization of silicate melts. Moreover in Fig. 9 we reported the calculated heat capacity using the Eq. 4 and data reported in Tab. 7. It should be noted that Fondo Riccio samples (FR) are not included in this parameterization because no molar absorptivity coefficients for molecular water and hydroxyl groups (ε_{5200} and ε_{4500}) are available in literature. The partial molar heat capacity of H_2O_{mol} and OH^- species appears to be dependent on chemical composition, increasing (CpH_2O_{mol}) and decreasing (Cp_{OH^-}) with the chemical parameter SM. The partial molar heat capacity of molecular water is indeed very small for all compositions investigated, with the highest Cp_{H2Omol} (21 J/mol K) showed by the most depolymerized sample (ETN). This could reflect the basically passive role of water molecules dispersed in the silicate network silicate structure. The PS sample, characterized by the lower network modifier content (16 mol %), shows the highest Cp_{OH^-} (~145 J/mol K) with respect to AMS-B1 (SM = 21 mol %; Cp_{OH^-} = 80 J/mol K) and ETN (SM = 32 mole%; Cp_{OH^-} = 68 J/mol K). This trend could be due to the different energy of interaction between hydroxyl groups and silicate network. $CpOH^-$ is higher for polymerized liquids as the dissolution of water into these melts strongly disrupts the structure creating a large number of configurational states. The energy needed to achieve these new configurational states is therefore higher compared to the case of the basalt, where an already depolymerized liquid interacts with water with weaker modification of its structure.

4.4 Configurational heat capacity of hydrous magmas

The heat capacity of a liquid is considered to be the sum of a vibrational and a configurational contribution. The configurational contribution on heat capacity [Cp^{conf} (T)] is a measure of the structural changes that occur on heating and represents the energy used to change the structure of a liquid in response to temperature variations. Assuming that the Cp_g (Tg), which represents the vibrational contribution to the heat capacity, do not vary significantly above the glass transition temperature (Richet and Bottinga, 1986), Cp^{conf} (T) can be taken as the difference between the heat capacity of the melt (Cp_{liq}) and the heat capacity of the glass at glass transition temperature [Cp_g (Tg)]:

$$Cp^{conf}(T) = Cp_{liq}(T) - Cp_g(Tg) \quad (5)$$

Fig. 10 shows the configurational heat capacities as a function of mole % H_2O for the studied liquids. As previously observed (Richet and Bottinga,1985; Bouhifd et al., 1998; Toplis et al., 2001; Webb, 2008), the Cp^{conf} (Tg) increases with decreasing SiO_2 content and increases with Al content and cation field strength of the atoms in the melt. Cp^{conf} (T) has contribution both chemical (related to all possible configurational states between oxygens and cations) and topological (distribution of TO distances and TOT angles) and the exact identification of the compositional dependence of these parameters is somewhat difficult. In general, the Cp^{conf} (T) increase with decreasing SiO_2 content (and decreasing of the SiO_2 / Al_2O_3 ratio) is ascribed to a general decrease of the overall strength of TO bonds, and to a correlated increase of the TO and TOT distribution (topological contribution to the configurational entropy).

The role of alkali versus alkaline earth cation and Al/Si order disorder is more complex. According to Webb (2008, and references therein) it is well known that the configurational heat capacities of the Na_2O–Al_2O_3–SiO_2 melts are lower than those of the CaO–Al_2O_3–SiO_2 melts. Explanations for

this behavior are various and are related to the differences between the field strength of these cations (Bouhifd et al., 1998). To understand how the Cp^{conf} (T) varies with composition, and hence silicate structure, we can refer to the fragility of silicates melts because it is well known that the configurational entropy affects the fragility of melts (e.g.,Toplis et al., 1997; Neuville, 2006; Webb et al., 2007; Webb, 2008; Di Genova et al., 2013). The fragility describes the departure of the liquid viscosity from an Arrhenian temperature dependence (Angell, 1991), and within the framework of Adam and Gibbs (1965) theory, is related to the temperature dependence of configurational entropy (S_c), which is in turn governed by the magnitude of the configurational heat capacity (Richet, 1984): $\log_{10}\eta(T) = A_e + \frac{B_e}{TS_c(T)}$ where A_e and B_e are temperature independent constants (Richet 1984).

Fragility can be expressed via the steepness index *m* (Plazek and Ngai, 1991; Bohmer and Angell, 1992) which describes the gradient of the viscosity curve at the glass transition temperature (Tg) on a reduced temperature scale:

$$m = \left.\frac{d(\log_{10}\tau)}{d\left(\frac{Tg}{T}\right)}\right|_{T=Tg} \quad (6)$$

where τ is the average relaxation time and Tg the glass transition temperature (at τ = 100 sec). The calculated values of fragility using viscosity measurements and Eq. (6) for our liquids are *m* = 46.1, 42.7, 25.3 and 24.8 for ETN, FR, AMS-B1 and PS melts respectively (Di Genova et al., 2013) . In Fig. 11 we report the calculated Cp^{conf} (Tg) for the melts studied in this work as a function of fragility. This figure shows that fragile melts have a higher configurational heat capacity compared to strong melts as predicted by the Adam and Gibbs (1965) theory. In general, many structural studies as well as molecular dynamic simulations, have suggested that alkaline-earth bearing liquids are more fragile than alkali-bearing liquids (Romano et al., 2001; Whittington et al., 2001; Neuville, 2006; Webb et al., 2007; Webb, 2008; Cheng et al., 2012; Di Genova et al., 2013). The high

electronegativity of the alkaline earth cations causes a general lengthening of the T-O average bond strength and a decrease in the mean TOT bond angle compared to the alkali-bearing case. Moreover, being divalent, the alkaline earth cations require two Al cations to be electrically balanced and the formation of Al-O-Al linkages further destabilizes the structure. The presence of divalent cations and the coupling of Al tetrahedral therefore imposes a strain in the network which facilitates its breakdown at high temperature, causing fragile behavior (Scamehorn and Angell, 1991). An increase of Al with respect to Si has a similar effect of lengthening TO bonds and decreasing TOT bond angle, thus destabilizing the network (Geisinger et al., 1985; Navrotsky et al., 1985). This is also consistent with observed structural changes in anorthite from room T to 1600°C (Taylor and Brown Jr., 1979; Okuno and Marumo, 1982) compared to no changes observed for albite from room to high T (Taylor et al., 1980; Okuno and Marumo, 1982). It has also been observed that highly electronegative cations tend to bond with nonbridging oxygen in the least polymerized Qn species available (Mysen, 1997), to minimize steric hindrance. Neuville, (2006) performed viscosity and RAMAN measurements in the SiO_2-Na_2O-CaO system and showed an increases in Q^2 and Q^4 species compared to Q^3 with increasing CaO content compared to Na_2O content.

Moreover, recent RAMAN structural studies from Cheng et al. (2012) for Na_2O-CaO-Al_2O_3-SiO_2 showed an increase in Q^2 species and a decrease in Q^3 species with the increase of Al/Si ratio. In general, for the same NBO/T, a shift to the right of the equilibrium $Q^3 \rightarrow Q^4 + Q^2$ can correlate to the overall stability of the network and its fragility as it has been long recognized that not all the Q^n species are energetically equivalent. In fact, it has been observed (Stebbins, 1987, Mysen, 2005) that T-NBO distances are longer in Q^2 species compared to Q^3 species, and an increase of Q^2 species can therefore lead to a general increase of the network distortion. A shift to the right of equilibrium $Q^3 \rightarrow Q^2 + Q^4$ can also increase the chemical contribution to the configuration heat capacity via an increase in Q species disorder.

In summary low silica content, high Al/Si ratio and Ca+Mg/Na+K ratio can increase the fragility via an increase in both chemical (Q species disorder, Al/Si OD) and topological (TO bond distances, TOT bond angles and TO and TOT distribution) disorder as registered by an equivalent increase in S_c and Cp^{conf}. The fragility of our samples can be easily explained in terms of different silica content, and different Al/Si and alkaline versus alkalies ratios. We observe a steady increase in fragility from PS (m=24.8) to AMS-B1 (m= 25.3) to FR (m=42) to ETN (m=46), accompanied to a general increase of Cp^{conf} (Tg) (PS= 11.2, AMS-B1=9.8; FR=16.4; ETN=22.4). A first-order parameter in increasing fragility in our liquids is the NBO/T (0.11; 0.10; 0.20; 0.45) and the silica content, gradually decreasing from PS to ETN. An increase in Al/Si ratio and in Ca+Mg/Na+K ratio from PS to AMS-B1, FR and ETN parallel the decrease in SiO_2 can further increase fragility and Cp in the same direction.

Although the trends observed can be easily interpreted in terms of chemistry and structural relationships, the extent of such variations are more difficult to be accounted for PS. PS pantelleritic liquid, with much higher SiO_2 content than AMS-B1, very low Ca+Mg/Na+K ratio and very low Al/Si would have expected to be much stronger than AMS-B1 liquid, whereas the difference in fragility is minor (24.8 versus 25.3) and Cp^{conf} (Tg) of PS is even slightly higher (11.2) compared to Cp^{conf} (Tg) of AMS-B1 (9.8). In contrast, there is a large increase in *m* and Cp^{conf} (Tg) from AMS-B1 to FR, despite the relatively small decrease in SiO_2, increase in Ca+Mg/Na+K and the same values for Al/Si. Obviously, as this important relationship brings to light, more structural and energetic parameters exists that should be taken into account to completely define the behaviour of these complex liquids. In Fig. 10 we report the variation of configurational heat capacity as a function of total water content. Also in this case a compositional dependence is apparent. For the most polymerized alkaline melts (AMS-B1 and PS) a slight increase of Cp^{conf} (Tg) can be observed as water is added to the melt. The increase in configurational heat capacity is consistent with the increases in fragility determined by viscosity measurements (Romano et al., 2001; Di Genova et al.,

2013). In Fig. 10 the variation of the Cp^{conf} (Tg) as a function of H_2O for the most depolymerized alkaline-earth melts (ETN and FR) is also reported. For these depolymerized compositions, after an initial increase up to ~6 mol% of water, the Cp^{conf} (Tg) strongly decreases as further H_2O is added to the melt, suggesting, opposite to the case for polymerized compositions, that water could decrease the fragility. In literature, the effect of H_2O on the melt fragility is still debated and both a decrease and an increase in fragility as a function of water content have been reported (Richet, et al., 1996; Whittington et al., 2000; Romano et al., 2001; Whittington et al., 2001; Bouhifd et al., 2012; Robert et al., 2012; Genova et al., 2013). We derived the fragility variations as a function of water content for FR (Misiti et al., 2011) and AMS-B1 (Romano et al., 2001; Misiti et al., 2006) only. For these two compositions, in fact, a complete data set of high-T, low-T, anhydrous and hydrous viscosity measurements exist and this allows to minimize errors included in the determination of fragility and hence possible artifacts in the results. In fact, as reported in Angell (2002), the value of the fragility (here defined as steepness index *m*, Eq. 6) obtained by a relatively small viscosity range near the glass transition temperature depends on the range of data fitted. For this reason, we chose not to include PS and ETN sample in the calculation, as for these two compositions hydrous viscosity data at high T are not available. Using the well-known three parameter Vogel- Fulcher-Tammann (VFT) equation to describe the temperature dependence of viscosity [$\log \eta = A + B / (T - C)$], the steepness index *m* can be expressed as reported as follow (Plazek and Ngai, 1992, Böhmer and Angell, 1992; Giordano and Dingwell, 2003b):

$$m = \frac{B}{T_{12}\left(1-\frac{C}{T_{12}}\right)^2} \quad (7)$$

where B and C are VFT parameters and T_{12} represents the temperature at which the viscosity (η) is equal to 10^{12} Pa sec. In order to evaluate the effect of water content on the B and C parameter, and

hence on the fragility (*m*) of the melts, we adopted a modified VFT equation reported in Di Genova et al. (2013):

$$\log \eta = A + \frac{[b_3 + b_4 \cdot \log (1+H_2O)]}{T - [c_3 + c_4 \cdot \log (1+H_2O)]} \quad (8)$$

Using Eq. 8 we parameterized the viscosity data by Misiti et al. (2011) for FR samples and by Romano et al. (2001) and Misiti et al., (2006) for AMS-B1 samples, and finally calculated the fragility using Eq. 7. In Tab. 8 fitting parameters for Eq. 8 are reported. In Tab. 9 and Fig. 12 the calculated fragility for the latite (FR) and trachyte (AMS-B1) liquids are reported as a function of water content. It is evident from Fig. 12 that water acts in different ways decreasing the fragility in the case of the FR latitic liquid, and increasing *m* for the AMS-B1 trachytic liquid. This different behavior might be related to the different dissolution mechanisms of water in silicate melts characterized by different chemical compositions (Giordano et al., 2009; Di Genova et al., 2013). Water dissolves in melts as both hydroxyl groups and molecular water reacting with the silicate network in different ways (Stolper, 1982a,b; Silver and Stolper 1985, 1989; Silver et al. 1990). According to the classical model of water dissolution (Burnham, 1975; Stolper, 1982a,b; Sykes and Kubicki, 1993, 1994; McMillan, 1994), water dissolves into polymerized compositions as AMS-B1 and PS melts creating NBOs in terms of SiOH and AlOH species and disrupting the silicate network. The depolymerization reaction not only decreases the overall T–O strength of the melt (increase in the topological contribution to Cp^{conf} and S_c) but also creates a large number of configurational states available for the activation of viscous flow (increase in the chemical contribution to the Cp^{conf} and S_c). As we observe in our measurements, the configurational heat capacity (and the configurational entropy) increases resulting in an increase in fragility, as derived for the AMS-B1 liquid.

For depolymerized melts, different reactions involving a polymerization of the silicate network and creation of free OH^- upon dissolution of water have been proposed (Fraser, 1977; Xue and Kanzaki, 2004, 2008; Moretti, 2005; Mysen and Cody, 2005). In principle, all the reactions, leading to either the polymerization or depolymerization of the silicate network, can operate simultaneously, and the net effect of water would depend on the predominance of one reaction over the others. In general, the polymerization reaction is expected to be more abundant in the presence of NBOs, and therefore on depolymerized melts, whereas the depolymerization reaction would be predominant in the opposite case of polymerized melts. The effect on fragility would also be opposite. In the case of depolymerized compositions, the polymerization induced by the dissolution of water would create a stronger melt, with fewer configurational states available for viscous flow and stronger T-BO bonds, decreasing Cp^{conf} and S_c and decreasing fragility, as observed for the FR liquid. For polymerized compositions, the depolymerization would increase the number of configurational states and increase fragility, as observed for AMS.

In conclusion the increase in Cp^{conf} (Tg) caused by water dissolution in trachyte is consistent with the fragility increases determined by viscosity data provided by Romano et al. (2001) and Misiti et al. (2006) and discussed in Giordano et al (2009), while the opposite behavior is observed for the more depolymerized liquid (FR).

5 Volcanological implications: eruptive thermal budget

Heat capacity represents a fundamental parameter to understand the evolution of multicomponent and multiphase equilibria energetics and therefore the kinetics and dynamics of igneous and volcanic processes. Transport properties of silicate melts, as thermal diffusivity (D = mm^2/s) and thermal conductivity (k = W/m K) represent the main properties controlling the kinetics of crystal growth and the conductive heat flow of a magmatic system, respectively. Thermal

diffusivity (D) is commonly expressed by the following equation (Snyder et al., 1994; Whittington et al., 2009):

$$D = k / \rho Cp \quad (9)$$

where k is thermal conductivity, ρ is density (Kg/m^3) and Cp is heat capacity (J/Kg m). As an example to demonstrate the need and importance of accurate Cp measurements, we calculated the thermal diffusivity of our Ca-Mg rich liquid composition (ETN and FR) using both the liquid heat capacity data presented in this paper and Cp values calculated by Stebbins et al. (1984) model for dry and hydrous conditions. We use liquid thermal conductivities provided by Snyder et al. (1994) on molten $CaMgSi_2O_6$ at T between 1673 and 1873 K. The calculated D using data presented in this work are always higher compared to the calculation performed using Stebbins et al. model (1984) with differences up to 12 % for the highest water content considered. Those differences are bound to influence significantly any model involving the flow of heat, as cooling of magma body, or convection and crystallization models.

In general, experimental data (e.g. Romine et al., 2012) demonstrate that the effect of T is much stronger on Cp than on ρ and D, and that therefore Cp variations, especially at the glass to liquid transition, are bound to influence thermal conductivity the most, making accurate measurements of Cp essential for proper calculation of thermal conductivity.

Heat capacity data are also essential to quantify magma degassing and heat flux during steady-state volcanic activity, which in turn control the style and energy of the eruption. White transient activity, for instance, the energy released by the expansion of the gas and by the cooling of magma juveniles, is converted into energy used to accelerate the gas and magma in the explosion, to raise the magmatic material within the gravity field, and to overcome the air drag acting on individual pieces of solid material. Harris and Stevenson (1997) presented a model for magma degassing in order to

constrain the steady-state magma system of Stromboli (Italy). In order to calculate the total thermal flux, the heat carried by expelled ejecta (Q_{ejecta}) during eruptions must be taken into account. Harris and Stevenson (1997) calculated Q_{ejecta} as follow:

$$Q_{ejecta} = (Cp\ \Delta T_e + C_L)\ M_e \quad (10)$$

where Cp is the heat capacity of ejecta (1150 J/kg J), ΔT_e is the ejecta cooling from eruption (1000 K) to room temperature, C_L is the latent heat of crystallization ($3*10^5$ J/kg) and M_e is the mass flux of erupted material (6 Kg/s). Using these data with Eq. 10 the authors calculated Q_{ejecta} = 8MW. Using the measured heat capacity in this work for anhydrous trachybasalt we obtain a dramatic increase of 38% in heat flux, that is Q_{ejecta} = 11 MW which results in a much stronger energy release and eruption energy. Proper assessment of heat capacity values, for glasses and liquids, for molten material and gases, are therefore pivotal to the modeling of the energy budget in a eruption, therefore defining eruptive style and hazard assessment issues.

6 Conclusions

Our study highlights a very complex energetic behavior for multicomponent hydrous silicate melts. In general, the anhydrous and hydrous heat capacities of glasses are in good agreement with previous studies confirms that the partial molar heat capacity of water is independent of glass composition, in a wide range of silicates ($0 \leq NBO/T \leq 1.5$).

Anhydrous liquid heat capacities are also well reproduced by literature models, considering a temperature dependence for $CpAl_2O_3$ as reported by Courtial and Richet (1993). The behavior of water in silicate liquids however is not reproduced by any current literature model. We derived partial molar CpH_2O of 41.38 J/mol K independent of composition for the natural liquids investigated. Partial molar heat capacities of molecular water and hydroxyl groups were also

derived for the compositions investigated in this study. We observed a dependence of partial molar heat capacity of molecular water and hydroxyl groups on composition, and parameterized it as a function of the structural parameter SM.

Anhydrous configurational heat capacity Cp^{conf} (Tg) and fragility (*m*) increases with decreasing SiO_2 and increasing Al content. We observed that alkaline-earth bearing (ETN and FR) liquids are more fragile than alkali-bearing liquids (AMS-B1 and PS). The effect of water on Cp^{conf} (Tg) and therefore on fragility was also parameterized in terms of composition. For the most polymerized melts (AMS-B1 and PS) a slightly increase of Cp^{conf} (Tg), and hence in fragility, can be observed as water is added to the melt, while for depolymerized compositions (ETN and FR) after a small initial increase, the C_p^{conf} (Tg) and fragility strongly decrease as further water is added to the melt. We argue that this behaviour might be related to the different dissolution mechanisms of the water in silicate melts characterized by different chemical compositions. The effect of water on the melt fragility would depend on the predominance of the different polymerization and/or depolymerization reactions.

The effect of water on magma fragility should also be taken into account when modeling degassing processes and eruption energy. In general, during degassing, magma viscosity increases and this leads to an exponential interrelated increase of degassing and viscosity up to fragmentation conditions. It is generally considered (Dingwell et al., 1996; Whittington et al., 2001; Vetere et al., 2006; Giordano et al., 2008; Misiti et al., 2011; Di Genova et al., 2013;) that the increase in viscosity due to degassing is stronger for polymerized compositions (rhyolites) than for depolymerized liquids (basalts), which translates into higher energy of degassing and fragmentation for the former. However, the trends reported in previous parameterizations could at least be in part affected by a lack of measurements in the hydrous high-T conditions and therefore by an incorrect estimate and modeling of fragility. When corrected for the increase in fragility at decreasing water content, as observed in our measurements of Cp for depolymerized liquids, the viscosity increase of

basalt during degassing may be more rapid than previously expected. Moreover, degassing induced crystallization is also known to be more pronounced for a basaltic composition (Applegarth et al., 2013), leading to a further increase in viscosity. The combined effects of degassing-induced crystallization and degassing induced increase in fragility, may be so strong to induce rapid rheological changes with temperature prone to affect the eruption dynamics.

Acknowledgements

We thank Dr. F. Bellatreccia and Prof. G. Della Ventura for FTIR analyses collected at the Laboratory of Infrared Spectroscopy, Department of Science, Roma Tre University. We wish to thank also M. Serracino for EMP analyses.

References

. Adam, G., Gibbs, J.H., (1965) On the temperature dependence of cooperative relaxation properties in glass-forming liquids. *J. Chem. Phys* **43**, 139-146.

Angell, C. A. (2002) Liquid fragility and the glass transition in water and aqueous solutions: *Chemical reviews*, **102** (8), 2627–50.

Applegarth, L.J., Tuffen, H., James, M.R., Pinkerton, H., (2013). Degassing-driven crystallisation in basalts: *Earth-Sci. Rev*. **116**, 1–16.

Behrens, H., Nowak, M., (2003) Quantification of H_2O speciation in silicate glasses and metls by IR spectroscopy - in situ versus quench techniques: *Phase Trans.***76**, 49, 45–61., doi: 10.1080/0141159031000076048.

Behrens, H., Stuke, A., (2003) Quantification of H_2O contents insilicate glasses using IR spectroscopy — a calibration based on hydrous glasses analyzed by Karl–Fischer ti- tration: *Glass Technol.* **76**, 176–189.

Behrens, H., Zhang, Y., (2009) H_2O diffusion in peralkaline to peraluminous rhyolitic melts: *Contrib. Mineral. Petrol.* **157**, 765–780, doi: 10.1007/s00410-008-0363-4.

Behrens, H., Romano, C., Nowak, M., Holtz, F., Dingwell, D.B., (1996) Near-infrared spectroscopic determination of water species in glasses of the system $MAlSi_3O_8$ (M= Li, Na, K): an interlaboratory study. *Chem. Geol*. **128**, 41 - 63.

Bouhifd, M.A., Courtial, P., Richet, P., (1998) Configurational heat capacities: alkali vs . alkaline-earth aluminosilicate liquids: *J. Non-Cryst. Solids* **231**, 169–177.

Bouhifd, M.A., Whittington, A., Roux, J., Richet, P., (2006) Effect of water on the heat capacity of polymerized aluminosilicate glasses and melts. *Geochim. Cosmochim. Acta* **70**, 3, 711–722., doi: 10.1016/j.gca.2005.09.012.

Bouhifd, M.A., Whittington, A., Withers, a. C., Richet, P., (2012) Heat capacities of hydrous silicate glasses and liquids: *Chem. Geol.*, **8**, doi: 10.1016/j.chemgeo.2012.10.026.

Burnham C. W. (1975) Water and magmas – mixing model: *Geochim. Cosmochim. Acta* **39**, 1077–1084.

Burnham, C.W., Davis, N.F., (1974) The role of H_2O in silicate melts: II. Thermodynamic and phase relations in the system $NaAlSi_3O_8$-H_2O to 10 kilobars, 700° to 1100°C: *Am J. Sci.* **274**, 902–940.

Böhmer, R., Angell, C.A., (1992) Correlations of the nonexponentiality and state dependence of mechanical relaxations with bond connectivity in Ge-As-Se supercooled liquids: *Phy. Rev. B* **45**, 17, 10091–10094.

Cheng, J.S., Xiao, Z., Yang, K., Wu, H., (2012) Viscosity, fragility and structure of Na_2O – CaO – Al_2O_3 – SiO_2 glasses of increasing Al / Si ratio: *Ceram. Int.* **39**, *4055-4062*.

Clemens J.D., Navrotsky A.N., (1987) Mixing properties of $NaA1Si_3O_8$ melt-H_2O: new calorimetric data and some geological implications. *J. Geol.* **95**, 173-186.

Courtial P., Richet P., (1993) Heat capacity of magnesium aluminosilicate melts. *Geochim. Cosmochim. Acta* **57**: 1267–1275.

Davis, M.J., Ihinger, P.D., Lasaga, A.C., (1997) Influence of water on nucleation kinetics in silicate melt: *J. Non-Cryst. Solids* **219**, 62–69, doi: 10.1016/S0022-3093(97)00252-4.

Dingwell, D.B., (2006) Transport Properties of Magmas: Diffusion and Rheology. *Elements*, **2**, 5, 281–286., doi: 10.2113/gselements.2.5.281.

Dingwell, D.B., Romano, C., Hess, K.-U., (1996) The effect of water on the viscosity of a haplogranitic melt under P-T-X conditions relevant to silicic volcanism: *Contrib. Mineral. Petrol.* **124**, 19–28.

Di Genova, D., Romano, C., Hess, K.-U., Vona, A., Poe, B.T., Giordano, D., Dingwell, D.B., Behrens, H., (2013) The rheology of peralkaline rhyolites from Pantelleria Island: *J. Volcanol. Geoth. Res.* **249**, 201–216.

Fanara, S., Behrens, H., Zhang, Y., (2012) Water diffusion in potassium-rich phonolitic and trachytic melts: *Chem. Geol.* **346**, 149-161 doi: 10.1016/j.chemgeo.2012.09.030.

Fenn, P.M., (1977) The nucleation and growth of alkali feldspars from hydrous melts: *Can. Mineral*. **15** , 2 , 135–161.

Fraser, D. G. (1977) Thermodynamic properties of silicate melts: *Thermodynamicsin Geology* (ed. D. G. Fraser). D. Reidel Pub. Co., Dortrecht-Holland, 301–325.

Geisinger, K.L., Gibbs, G. V, Navrotsky, A., (1985) A molecular orbital study of bond length and angle variations in framework structures: *Phys. Chem. Min.* **11**, 6, 266–283 LA – English, doi: 10.1007/BF00307405.

Ghiorso, M.S., Sack, R.O., (1995) Chemical mass transfer in magmatic processes IV. A revised and internally consistent thermodynamic model for the interpolation and extrapolation of liquid-solid equilibria in magmatic systems at elevated temperatures and pressures: *Contrib. Mineral. Petrol.* **119**, 2-3, 197–212, doi: 10.1007/BF00307281.

Giordano, D., Dingwell, D. B. (2003a) Viscosity of hydrous Etna basalt: implications for Plinian-style basaltic eruptions: *Bull. Volcanol.* **65**, 8–14.

Giordano, D., Dingwell, D.B., (2003b) The kinetic fragility of natural silicate melts: *J. Phys. Cond. Mat.* **15**, S945–S954.

Giordano, D., Nichols, A.R.L., Dingwell, D.B., (2005) Glass transition temperatures of natural hydrous melts: a relationship with shear viscosity and implications for the welding process: *J. Volcanol. Geoth. Res.* **142**, 105–118, doi: 10.1016/j.jvolgeores.2004.10.015.

Giordano, D., Mangiacapra, A., Potuzak, M., Russel, J.K., Romano, C., Dingwell, D.B., Di Muro, A (2006) An expanded non Arrehenian model for silicate melt viscosity: a treatment for metaluminous, peraluminous, and peralkaline liquids: *Chem. Geol.* **229**, 42-56.

Giordano, D., Potuzak, M., Romano, C., Dingwell, D.B., Nowak, M., (2008) Viscosity and glass transition temperature of hydrous melts in the system $CaAl_2Si_2O_8$ - $CaMgSi_2O_6$: *Chem. Geol.*, **256**, 203–215, doi: 10.1016/j.chemgeo.2008.06.027.

Giordano, D., Ardia, P., Romano, C., Dingwell, D. B., Di Muro, A., Schmidt, M. W., Mangiacapra, A., et al. (2009) The rheological evolution of alkaline Vesuvius magmas and comparison with alkaline series from the Phlegrean Fields, Etna, Stromboli and Teide. *Geochim. Cosmochim. Acta*, **73**, 6613–6630 doi:10.1016/j.gca.2009.07.033.

Harris, A.J.L., Stevenson, D.S., (1997) Magma budgest and steady-state activity of Vulcano and Stromboli: *Geophys. J. Roy. Astron. Soc.* **24**, 9, 1043–1046.

Iacono-Marziano, G., Morizet, Y., Trong, E. Le, Gaillard, F., (2012) New experimental data and semi-empirical parameterization of H_2O-CO_2 solubility in mafic melts: *Geochim. Cosmochim. Acta* **97**, 1-23, doi: 10.1016/j.gca.2012.08.035.

James, M.R., Lane, S.J., Wilson, L., Corder, S.B., (2009) Degassing at low magma-viscosity volcanoes: Quantifying the transition between passive bubble-burst and Strombolian eruption: *J. Volcanol. Geoth. Res.* **180**, 2-4, 81–88, doi: 10.1016/j.jvolgeores.2008.09.002.

Lange, R.L., Carmichael, I.S.E., (1990) Thermodynamic properties of silicate liquids with emphasis on density, thermal expansion and compressibility: *Reviews in Mineralogy and Geochemistry* **24**, 1, 25–64.

Lange, R.A., Navrotsky, A., (1992) Mineralogy and Heat capacities of Fe_2O_3-bearing silicate liquids: *Contrib. Mineral. Petrol.* **110**, 311–320.

Lange, R.A., Navrotsky, A., (1993) Heat capacities of TiO_2-bearing silicate liquids : Evidence for anomalous changes in configurational entropy with temperature: *Geochim. Cosmochim. Acta* **57**, 3001–3011.

Lesne, P., Scaillet, B., Pichavant, M., Iacono-Marziano, G., and Beny, J.M., (2011) The H_2O solubility of alkali basaltic melts : an experimental study: *Contrib. Mineral. Petrol.* **162**, 133–151, doi: 10.1007/s00410-010-0588-x.

McMillan P. F. (1994) Water solubility and speciation models: Volatiles Magmas **30**, 131–156.

Mercier, M., Di Muro, A., Giordano, D., Métrich, N., Lesne, P., Pichavant, M., Scaillet, B., Clocchiatti, R., Montagnac, G., (2009) Influence of glass polymerisation and oxidation on micro-Raman water analysis in alumino-silicate glasses: *Geochim. Cosmochim. Acta* **73**, 197–217, doi: 10.1016/j.gca.2008.09.030.

Misiti, V., Freda, C., Taddeucci, J., Romano, C., Scarlato, P., Longo, A., Papale, P., Poe, B.T., (2006) The effect of H_2O on the viscosity of K-trachytic melts at magmatic temperatures. *Chem. Geol.* **235**, 124–137.

Misiti V., Vetere F., Freda C., Scarlato P., Behrens H., Mangiacapra A., Dingwell D.B., (2011) A general viscosity model of Campi Flegrei (Italy) melts: *Chem. Geol.* **235**, 50–59.

Moretti, R., Papale, P., (2004) On the oxidation state and volatile behavior in multicomponent gas–melt equilibria: *Chem. Geol.* **213**, 1–3, 265–280.

Muncill, G., Lasaga, A.C.,(1988) Crystal-growth kinetics of plagioclase in igneous systems : Isothermal HrO-saturated experiments and extension of a growth model to complex silicate melts: *Am. Mineral.* **73**, 982–992.

Mysen, B. O., (1995) Structural behavior of Al^{3+} in silicate melts: In-situ, high-temperature measurements as a function of bulk chemical composition, *Geochim. Cosmochim. Acta* **59**, 455-474.

Mysen, B.O., (1997) Aluminosilicate melts: structure, composition and temperature: *Contrib. Mineral. Petrol.* **127**, 1-2, 104–118 LA – English, doi: 10.1007/s004100050268.

Mysen, B. O., Cody, G. D., (2005) Solution mechanisms of H_2O in depolymerised peralkaline melts: *Geochim. Cosmochim. Acta* **69**, 5557–5566.

Mysen, B. O., Toplis, M. J. (2007) Structural behavior of Al^{3+} in peralkaline, metaluminous, and peraluminous silicate melts and glasses at ambient pressure: *Am. Mineral.* **92** (5-6), 933–946. doi:10.2138/am.2007.2334.

Mysen, O., Virgo, D., Seifert, A., (1982) Implications for Chemical and Physical Properties of Natural Magma. *Rev. Geophysics Space Physics* **20**, 353-383.

Navrotsky, A., Geisinger, K.L., McMillan, P., Gibbs, G. V, (1985) The tetrahedral framework in glasses and melts — inferences from molecular orbital calculations and implications for structure, thermodynamics, and physical properties. *Phys. Chem. Min.*, **11**, 6, 284–298.

Neuville, D.R., (2006) Viscosity, structure and mixing in (Ca, Na) silicate melts: *Chem. Geol.*, **229**, 1–3, 28–41.

Nowak, M., Behrens, H., (1997) An experimental investigation on diffusion of water in haplogranitic melts: *Contrib. Mineral. Petrol.* **126**, 365–376.

Ochs F.A., Lange R.A. (1999) The density of hydrous magmatic liquid. *Science* **283**: 1314-1317

Okuno., M., Marumo F., (1982) The structures of anorthite and albite melts: *Min. J.* **11**, 4, 180–196.

Ohlhorst, S., Behrens, Holtz, F. 2001. Compositional dependence of molar absorptivities of nearinfrared OH^- and H_2O bands in rhyolitic to basaltic glasses. *Chem. Geol*. **174**, 5 - 20.

Papale, P., (1997) Modeling of the solubility of a one-component H_2O or CO_2 fluid in silicate liquids: *Contrib. Mineral. Petrol.* **126**, 3, 237–251, doi: 10.1007/s004100050247.

Papale, P., (1999) Strain-induced magma fragmentation in explosive eruptions. *Nature* **397**, 425–428.

Papale, P., Moretti, R., Barbato, D., (2006) The compositional dependence of the saturation surface of $H_2O + CO_2$ fluids in silicate melts: *Chem. Geol.* **229**, 1-3, 78–95, doi: 10.1016/j.chemgeo.2006.01.013.

Persikov, Y.S., Zharikov, V.A., Bukhtiyarov, P.G., Polskoy, S.F., (1990) The effect of volatiles on the properties of magmatic melts: *Europ. J. Min.* , **2**, 5, 621–642.

Plazek D. J. Ngai K. L. (1991) Correlation of polymer segmental chain dynamics with temperature-dependent timescale shifts: *Macromolecules* **24**, 1222–1224.

Richet, P., (1984) Viscosity and configurational entropy of silicate melts: *Geochim. Cosmochim. Acta* **48**, 471–483, doi: 10.1016/0016-7037(84)90275-8.

Richet, P., (1987) Heat capacity of silicate glasses. *Chem. Geol.***62**, 1-2, 111–124, doi: 10.1016/0009-2541(87)90062-3.

Richet, P., Bottinga, Y., (1985) Heat capacity of aluminum-free liquid silicates: *Geochim. Cosmochim. Acta* **49**, 2, 471–486, doi: 10.1016/0016-7037(85)90039-0.

Richet, P., Bottinga, Y., (1986) Thermochemical properties of silicate glasses and liquids: A review: *Rev. of Geophys.* **24**, 1, 1–25, doi: 10.1029/RG024i001p00001.

Richet, P., Neuville, D. R., (1992) Thermodynamics of silicate melts; configurational properties. In "Thermodynamic data; systematics and estimation", *Springer*, **10** (ed. S. K. Saxena), pp. 132-161.

Richet, P., Lejeune, A.M., Holz, F., Roux, J., (1996) Water and viscosity of andesite melts: *Chem. Geol*, **128**, 185–197.

Richet, P., Bouhifd, M.A., Courtial, P., Tequi, C., (1997) Configurational heat capacity and entropy of borosilicate melts: *J. Non-Cryst. Solids* **211**, 3, 271–280.

Richet, P., Hovis, G., Whittington, A. (2006). Water and magmas : Thermal effects of exsolution. *Earth Planet. Sci. Lett.* **241**, 972–977. doi:10.1016/j.epsl.2005.10.015.

Robert, G., Whittington, A., Stechern, A., Behrens, H., (2012) The effect of water on the viscosity of a synthetic calc-alkaline basaltic andesite: *Chem. Geol.* **1**–14, doi: 10.1016/j.chemgeo.2012.10.004.

Robie R. A., Hemingway B. S., and Fisher J. R. (1979) Thermodynamic properties of minerals and related substances at 298.5 K and 1 bar (10 Pascals) and at higher temperatures: *U.S.Geological Survey bulletin*. **1452**, 428 - 446.

Romano, C., Dingwell, D.B., Behrens, H., (1995) The temperature dependence of the speciation of water in $NaAlSi_3O_8$-$KAlSi_3O_8$ melts: an application of fictive temperatures derived from synthetic fluid-inclusions: *Contrib. Mineral. Petrol.* **122**, 1–10.

Romano, C., Poe, B.T., Mincione, V., Hess, K.-U., Dingwell, D.B., (2001) The viscosities of dry and hydrous $XAlSi_3O_8$ (X = Li, Na, K, Ca-0.5, Mg-0.5) melts: *Chem. Geol.*, **174**, 115–132.

Romine, W.L., Whittington, A., Nabelek, P.I., Hofmeister, A.M., (2012) Thermal diffusivity of rhyolitic glasses and melts: effects of temperature, crystals and dissolved water: *Bull. Volcanol.* **74**, 10, 2273–2287, doi: 10.1007/s00445-012-0661-6.

Scamehorn, C.A., Angell, C.A., (1991) Viscosity-temperature relations and structure in fully polymerized aluminosilicate melts from ion dynamics simulations: *Geochim. Cosmochim. Acta*, **55**, 3, 721–730, doi: http://dx.doi.org/10.1016/0016-7037(91)90336-4.

Shen, A., Keppler, H., (1995) Infrared spectroscopy of hydrous silicate melts to 1000 °C and 10 kbar: Direct observation of HrO speciation in a diamond-anvil cell: *Am. Mineral.* **80**, 1335–1338.

Silver, L.A., E.M. Stolper (1985) A thermodynamic model for hydrous silicate melts: *J. Geol.*, **93**, p. 161-178.

Silver, L.A., E.M. Stolper (1989) Water in albitic glasses: *J. Petrol.*, **30**, p. 667-709.

Silver, L.A., P.D. Ihinger, and E.M. Stolper (1990) The influence of bulk composition on the speciation of water in silicate glasses: *Contrib. Mineral. Petrol.*, **104**, p. 142-162.

Snyder, D., (2000) Thermal effects of the intrusion of basaltic magma into a more silicic magma chamber and implications for eruption triggering: *Earth Planet. Sci. Lett.*, **175**, 257–273.

Snyder, D., Gier, E.J., Carmichael, I.S.E., (1994) Experimental determination of the thermal conductivity of Molten $CaMgSi_2O_6$ and the transport of heat through magmas: *J. Geophys. Res.* **99**, , 15,503–15,516.

Spera, F.J., (2000) Physical properties of magma. In Encyclopedia on Volcanoes (*Sigurdsson, H. Ed.*). Academic Press, San Diego, California, 171-190.

Stebbins J.F. (1987) Identification of multiple structural species in silicate glasses by ^{29}Si NMR. *Nature* **330**, 465-467.

Stebbins, J.F., Carmichael, I.S.E., Moret, L.K., (1984) Heat capacities and entropies of silicate liquids and glasses: *Contrib. Mineral. Petrol.* **86**, 2, 131–148, doi: 10.1007/BF00381840.

Stolper, E.M., (1982a) Water in silicate glasses: An infrared spectroscopic study: *Contrib. Mineral. Petrol.* **81**, 1, 1–17 LA – English, doi: 10.1007/BF00371154.

Stolper E. M., (1982b) The speciation of water in silicate melts. *Geochim. Cosmochim. Acta* **46**, 2609–2620.

Sykes D. and Kubicki J. D. (1993) A model for H_2O solubility mechanisms in albite melts from infrared-spectroscopy and molecular-orbital calculations: *Geochim. Cosmochim. Acta* **57**, 1039–1052.

Sykes D. and Kubicki J. D. (1994) A model for H_2O solubility mechanisms in albite melts from infrared-spectroscopy and molecular-orbital calculations – reply. *Geochim. Cosmochim. Acta* **58**, 1381–1384.

Taylor, M., Brown Jr., G.E., (1979) Structure of mineral glasses—I. The feldspar glasses $NaAlSi_3O_8$, $KAlSi_3O_8$, $CaAl_2Si_2O_8$: *Geochim. Cosmochim. Acta* **43**, 1, 61–75, doi: http://dx.doi.org/10.1016/0016-7037(79)90047-4.

Taylor, M., Brown Jr, G.E., Fenn, P.M., (1980) Structure of mineral glasses—III. $NaAlSi_3O_8$ supercooled liquid at 805°C and the effects of thermal history: *Geochim. Cosmochim. Acta*, **44**, 1, 109–117, doi: http://dx.doi.org/10.1016/0016-7037(80)90181-7.

Toplis, M.J., Dingwell, D.B., Hess, K.-U., Lenci, T., (1997) Viscosity, fragility, and configurational entropy of melts along the join SiO_2-$NaAlSiO_4$: *Am. Mineral.* **82**, 979–990.

Toplis, M.J., Gottsmann, J., Knoche, R., Dingwell, D.B., (2001) Heat capacities of haplogranitic glasses and liquids: *Geochim. Cosmochim. Acta* **65**, 1985 - 1994.

Vetere, F., Behrens, H., Misiti, V., Ventura, G., Holtz, F., De Rosa, R., Deubener, J., (2007) The viscosity of shoshonitic melts (Vulcanello Peninsula, Aeolian Islands, Italy): Insight on the magma ascent in dikes: *Chem. Geol.*, **245**, 89–102, doi: 10.1016/j.chemgeo.2007.08.002.

Vona, A., Romano, C., (2013) The effects of undercooling and deformation rates on the crystallization kinetics of Stromboli and Etna basalts. *Contrib. Mineral. Petrol*. On line.

Vona, A., Romano, C., Dingwell, D.B., Giordano, D., (2011) The rheology of crystal-bearing basaltic magmas from Stromboli and Etna: *Geochim. Cosmochim. Acta*, **75**, 11, 3214–3236, doi: 10.1016/j.gca.2011.03.031.

Webb, S.L., (2008) Configurational heat capacity of Na_2O – CaO – Al_2O_3 – SiO_2 melts: *Chem. Geol.* **256**, 91–100, doi: 10.1016/j.chemgeo.2008.04.003.

Webb, S.L., Banaszak, M., Köhler, U., Rausch, S., Raschke, G., (2007) The viscosity of Na_2O-CaO-Al_2O_3-SiO_2 melts: *Europ. J. Min.*, **19**, 5, 681–692.

Whittington, A., Richet, P., Holtz, F., (2000) Water and the viscosity of depolymerized aluminosilicate melts: *Geochim. Cosmochim. Acta* **64**, **21**, 3725–3736.

Whittington, A., Richet, P., Linard, Y., Holtz, F., (2001) The viscosity of hydrous phonolites and trachytes: *Chem. Geol.* **174**, 209–223.

Whittington, A., Bouhifd, M. A., Richet, P. (2009) The viscosity of hydrous $NaAlSi_3O_8$ and granitic melts: Configurational entropy models. *Am. Mineral.*, **94** (1), 1–16. doi:10.2138/am.2009.2892.

Xue X., (2009) Water speciation in hydrous silicate and aluminosilicate glasses : Direct evidence from ^{29}Si-^{1}H and ^{27}Al-^{1}H double-resonance NMR*: Am. Mineral.* **94**, **3**, 395–398, doi: 10.2138/am.2009.3088.

Xue X. Y., Kanzaki M. (2004) Dissolution mechanisms of water in depolymerised silicate melts: constraints from H-1 and Si-29 NMR spectroscopy and ab initio calculations: *Geochim. Cosmochim. Acta* **68**, 5027–5057.

Xue X., Kanzaki M. (2008) Structure of Hydrous Aluminosilicate Glasses along the Diopside–Anorthite Join: A Comprehensive One- and Two-dimensional ^{1}H and ^{27}Al NMR Study. *Elsevier*.

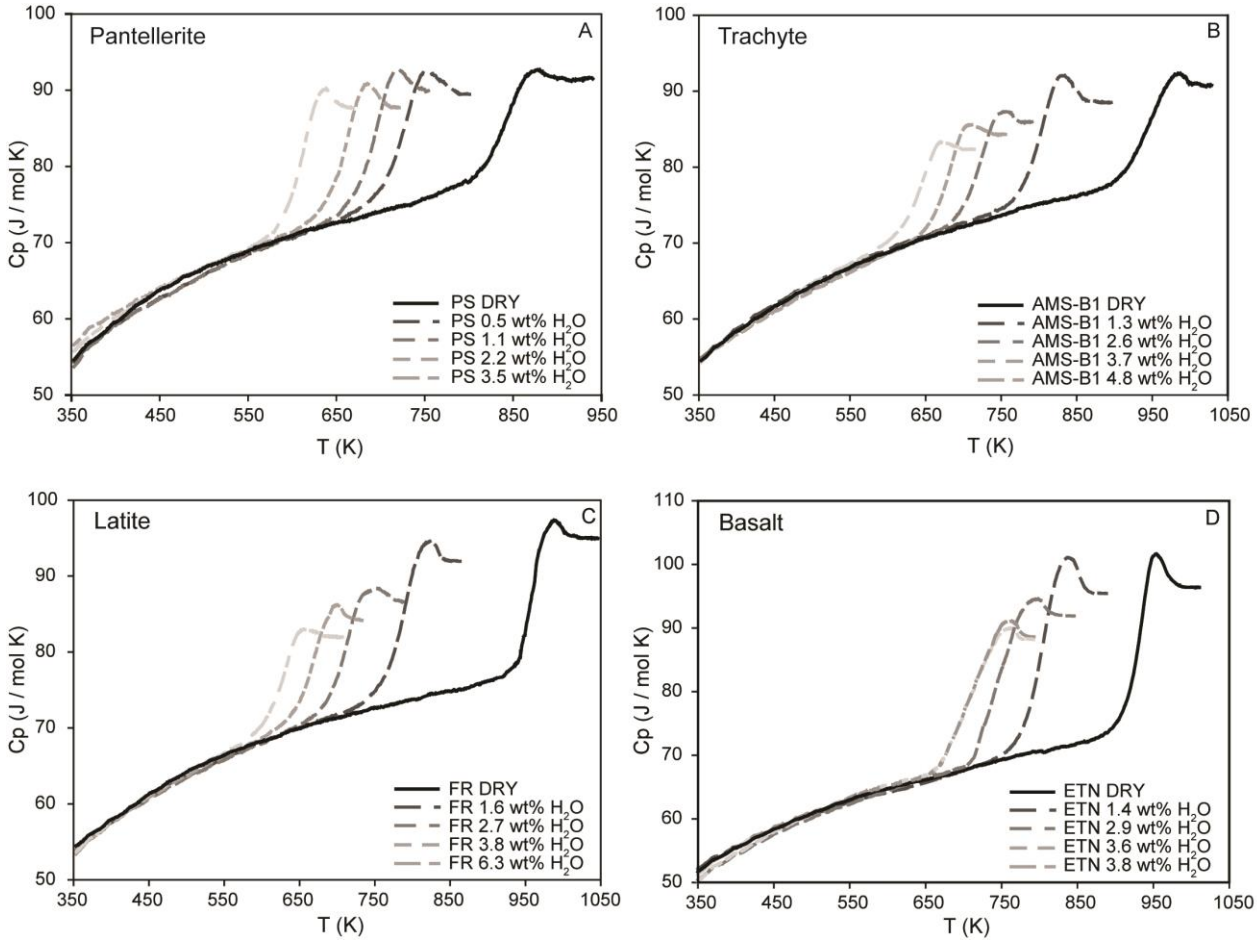

Fig.1: Measured heat capacity for (A) PS pantellerite, (B) AMS-B1 trachyte, FR latite and ETN basalt.

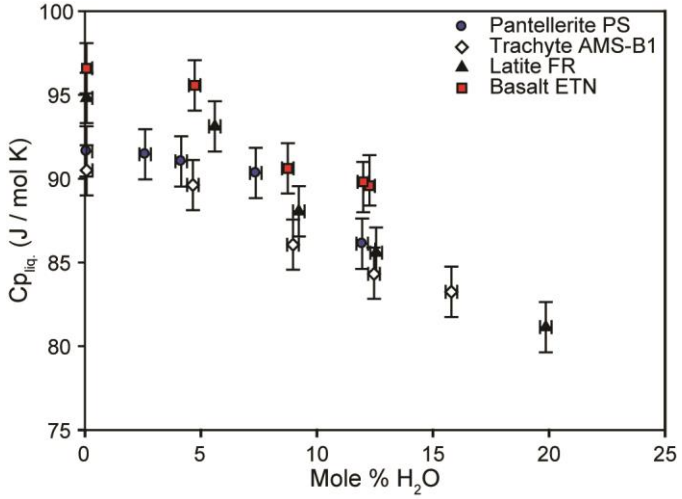

Fig.2: Measured heat capacity for the selected samples as a function of water content.

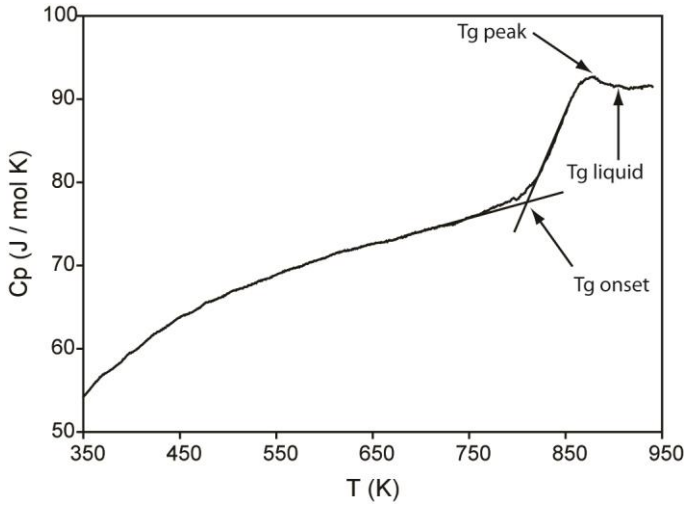

Fig.3: Measured heat capacity (Cp) for dry pantellerite sample (PS DRY) after cooling and heating at 20 K/min. In figure are shown the selected glass transition temperatures: Tg_{onset}, Tg_{peak} and $Tg_{liq.}$

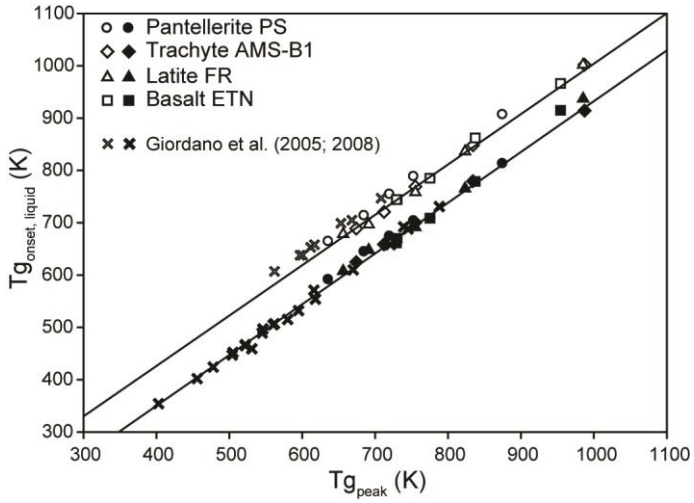

Fig.4: Comparison between measured glass transition temperatures in this study and reported in Giordano et al. (2005, 2008) as taken at onset, peak and stable liquid position of the Cp curves. Dark symbols represent the Tg_{onset} while the empty symbols represent $Tg_{liq.}$.

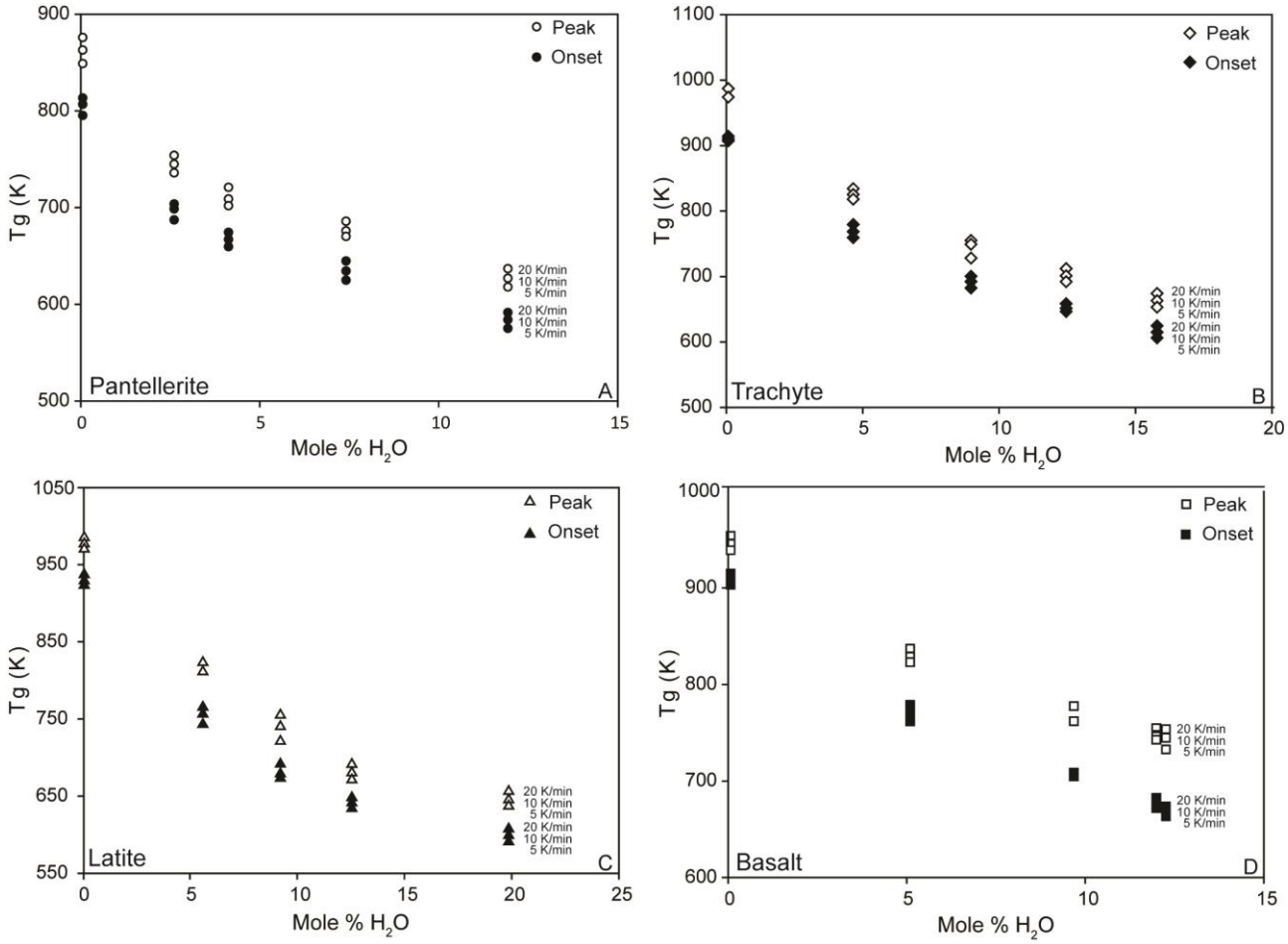

Fig.5: Measured Tg_{peak} as a function of different water content. The numbers reported in figures (20-10-5) indicate the different cooling-heating thermal treatment adopted in Cp measurements.

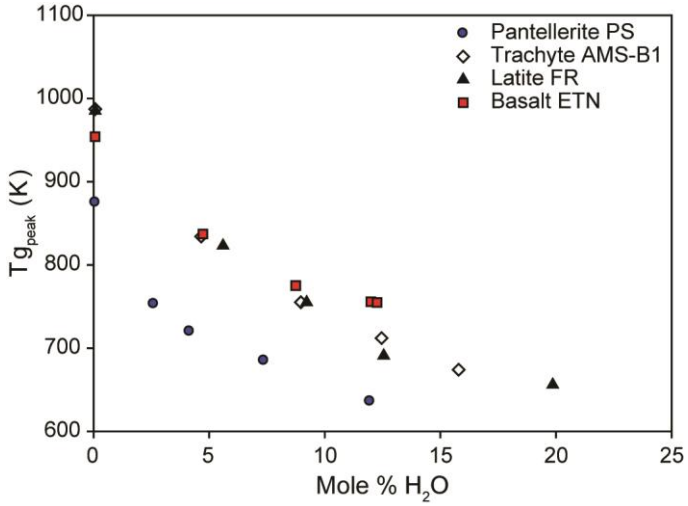

Fig.6: Effect of water on measured Tg_{peak} after cooling and heating at 20 K/min. The glass transition temperatures for pantelleritic melts are significantly lower (~100 K) than the measured Tg_{peak} for AMS-B1, FR and ETN samples.

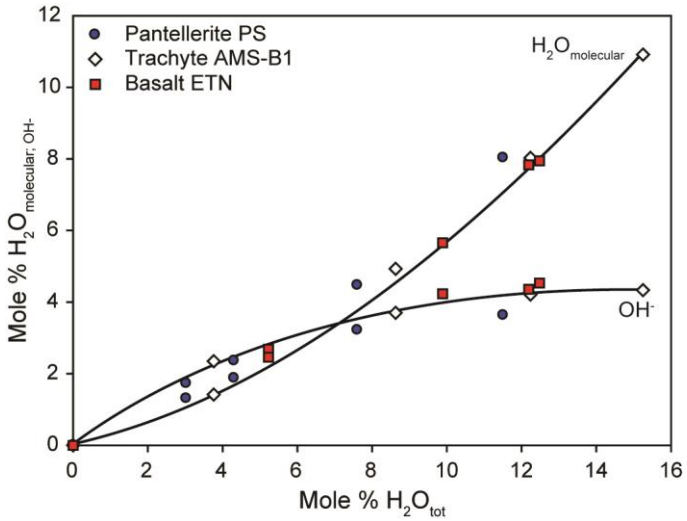

Fig.7: Measured water speciation in quenched hydrous glasses as determined from infrared spectroscopy measurements.

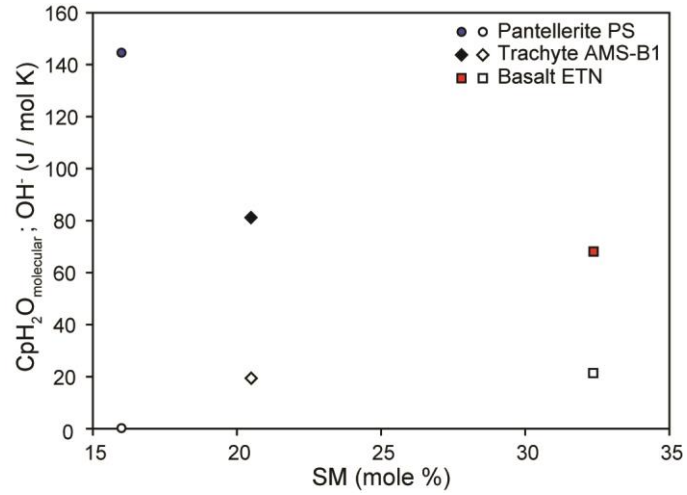

Fig.8: Calculated partial molar heat capacity of H_2O_{mol} and OH^- species using Eq. 4 as a function of SM parameter. Filled symbols refer to Cp_{OH^-}, while empty symbols represent the $Cp_{H2O\ mol.}$

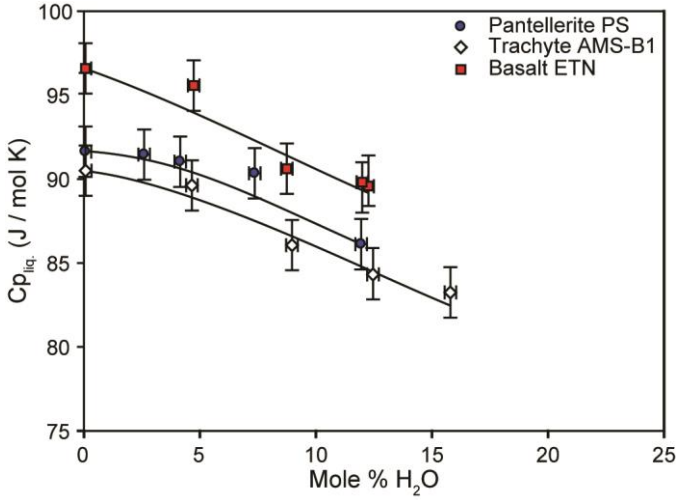

Fig. 9: Heat capacities of hydrous liquids ($Cp_{liq.}$) as a function of water content. Lines show the calculated heat capacities for liquids using Eq. 4 and measured partial molar heat capacities of OH^- and H_2O_{mol}.

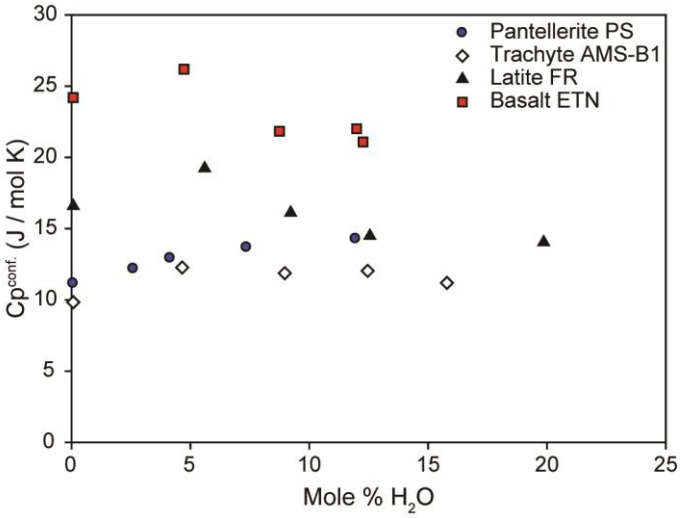

Fig.10: Configurational heat capacities at glass transition temperature of the melts investigated in this work as a function of water content.

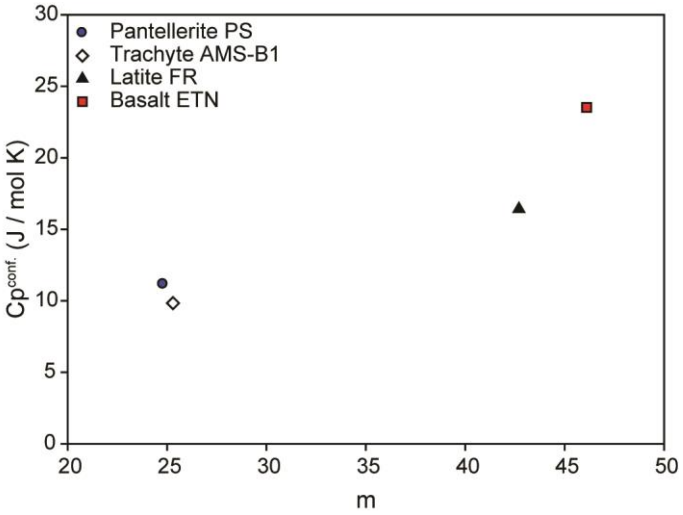

Fig.11: Configurational heat capacities at glass transition temperature of the melts investigated in this work as a function of fragility (m).

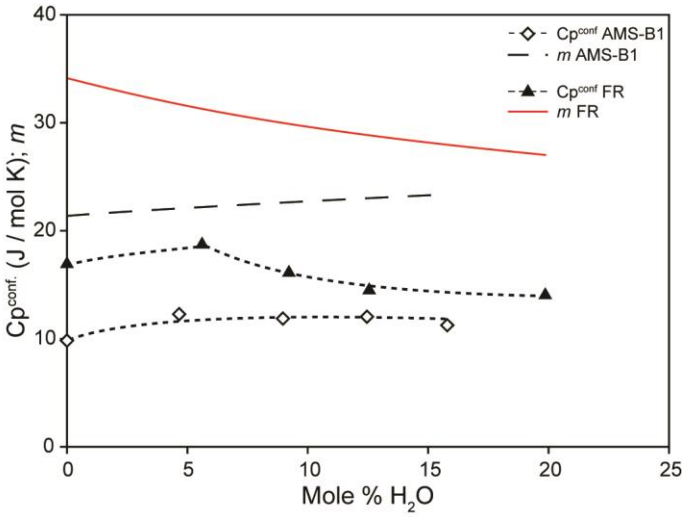

Fig. 12: Configurational heat capacities at glass transition temperature [Cp^{conf} (Tg)] and fragility (*m* defined by Eq. 7) as a function of water content.

Table 1

Dry composition (mol %) of glasses

	PS	AMS-B1	FR	ETN
SiO_2	77.76 (±0.27)	65.43 (±0.21)	62.33 (±0.24)	52.48 (±0.16)
TiO_2	0.41 (±0.4)	0.33 (±0.02)	0.68 (±0.05)	1.37 (±0.06)
Al_2O_3	5.96 (±0.05)	12.29 (±0.07)	11.68 (±0.06)	10.76 (±0.12)
FeO_{TOT}	5.21 (±0.15)	4.28 (±0.05)	6.16 (±0.09)	9.06 (±0.17)
Fe_2O_3	2.30 (±0.15)	-	-	-
FeO	3.14 (±0.11)	-	-	-
MnO	0.36 (±0.06)	0.10 (±0.02)	0.16 (±0.04)	0.23 (±0.03)
MgO	0.13 (±0.02)	2.47 (±0.03)	3.95 (±0.06)	8.89 (±0.09)
CaO	0.68 (±0.06)	5.14 (±0.06)	6.60 (±0.11)	11.73 (±0.11)
Na_2O	6.29 (±0.09)	4.09 (±0.06)	4.92 (±0.08)	3.90 (±0.09)
K_2O	2.89 (±0.09)	5.71 (±0.05)	3.21 (±0.09)	1.28 (±0.05)
P_2O_5	-	0 (±0.00)	0.22 (±0.04)	0.26 (±0.06)
gfw (g)[a]	66.40	67.20	66.15	64.39
N[b]	3.12	3.13	3.07	2.93

[a] Gram formula weight on the basis of one mole of oxides.

[b] Number of atoms per gfw.

Fe^{2+}/Fe^{tot} ratio of PS was measured by redox titration as reported in Di Genova et al. (2013).

Table 2

Measured water contents (FTIR and KFT), synthesis condition (pressure and temperature) of the hydrous samples and room temperature density of hydrated samples.

Sample	FTIR[a]		KFT[b]	P	T	ρ
	$H_2O_{molec.}$	OH^-	H_2O	(kbar)	(K)	(g l^{-1})
PS 0.5	1.38 (±0.04)	1.65 (±0.06)	2.6 (±0.15)	4	1473	2522 (±1)
PS 1.1	1.95 (±0.06)	2.36 (±0.09)	4.15 (±0.26)	4	1473	2507 (±1)
PS 2.2	4.47 (±0.13)	3.14 (±0.11)	7.36 (±0.21)	4	1473	2473 (±4)
PS 3.5	8.03 (±0.19)	3.48 (±0.14)	11.95 (±0.27)	4	1473	2420 (±2)
AMS-B1 1.3	1.42 (±0.06)	2.35 (±0.07)	4.66 (±0.26)	2.5	1373	2515 (±2)
AMS-B1 2.6	4.93 (±0.09)	3.70 (±0.06)	8.97 (±0.30)	2.5	1373	2472 (±1)
AMS-B1 3.7	8.03 (±0.17)	4.21 (±0.12)	12.46 (±0.27)	2.5	1373	2464 (±3)
AMS-B1 4.8	10.92 (±0.21)	4.33 (±0.13)	15.79 (±0.34)	2.5	1373	2418 (±2)
FR 1.6	-	-	5.6 (±0.19)	2.5	1473	-
FR 2.7	-	-	9.22 (±0.21)	2.5	1473	-
FR 3.8	-	-	12.55 (±0.16)	2.5	1473	-
FR 6.3	-	-	19.86 (±0.25)	2.5	1473	-
ETN 1.4	2.44 (±0.04)	2.59 (±0.06)	4.73 (±0.16)	2.5	1473	2760 (±1)
ETN 2.9	5.46 (±0.19)	4.23 (±0.13)	8.75 (±0.13)	2.5	1473	2741 (±2)
ETN 3.6	7.83 (±0.16)	4.36 (±0.11)	11.99 (±0.17)	2.5	1473	2719 (±3)
ETN 3.8	7.95 (±0.13)	4.53 (±0.12)	12.26 (±0.16)	2.5	1473	2718 (±2)

[a] Water content (mol%) measured by Infrared.spectroscopy.

[b] Water content (mol%) measured by Karl-Fischer titration (KFT).

Molar absorption coefficients for the combination band of OH^- at 4500 cm^{-1} and H_2O_m at 5200 cm^{-1}: PS (Behrens and Zhang, 2009), AMS-B1 (Misiti et al., 2006) and ETN (Lesne et al., 2011).

The duration of each experiment is 24 h.

Table 3

Measured glass transition temperatures (onset, peak, liquid) and liquid, glass and configuration heat capacites of the studied samples.

	T_g^{onset} (K)			T_g^{peak} (K)			T_g^{liquid} (K)					
Sample	20 (K/min)	10 (K/min)	5 (K/min)	20 (K/min)	10 (K/min)	5 (K/min)	20 (K/min)	10 (K/min)	5 (K/min)	$C_{pliq.}$[a]	C_{pg} (Tg_{onset})[a]	$C_{pconf.}$[a]
PS DRY	813	806	794	875	862	848	906	892	876	91.6	80.5	11.2
PS 0.5	703	698	686	753	744	735	788	766	753	91.5	79.3	12.2
PS 1.1	674	666	659	720	708	701	754	733	723	91.0	78.1	12.9
PS 2.2	644	634	624	685	675	669	713	691	-	90.3	76.7	13.7
PS 3.5	591	583	574	636	626	617	664	647	-	86.1	71.8	14.3
AMS-B1 DRY	914	910	907	987	974	974	1002	987	978	89.4	79.5	9.8
AMS-B1 1.3	779	768	759	834	825	818	848	848	834	89.6	77.3	12.3
AMS-B1 2.6	700	692	682	755	749	728	769	755	740	86.1	74.2	11.9
AMS-B1 3.7	659	651	647	712	701	692	721	708	709	84.3	72.3	12.0
AMS-B1 4.8	625	615	606	674	663	653	689	676	666	83.2	72.2	11.0
FR DRY	937	929	923	985	977	970	1002	993	984	94.8	78.4	16.4
FR 1.6	765	756	743	823	811	811	836	832	831	93.1	73.9	19.2
FR 2.7	691	679	673	755	740	721	758	742	726	88.1	71.9	16.1
FR 3.8	648	641	634	691	680	671	696	695	677	85.6	71.1	14.5
FR 6.3	608	599	591	656	645	637	678	649	642	81.1	67.1	14.0
ETN DRY	915	909	903	954	946	939	966	-	-	96.6	72.2	24.4
ETN 1.4	779	769	762	837	829	823	862	858	-	95.6	68.6	26.9
ETN 2.9	709	707	705	775	760	753	785	-	-	91.1	68.9	22.2
ETN 3.6	663	656	654	760	753	748	778	-	-	90.4	68.1	22.3
ETN 3.8	661	655	651	759	750	745	775	-	-	89.5	67.6	21.9

[a] Data in J mol^{-1} K^{-1}

Table 4
Coefficients for the Maier Kelley equation (Eq. 1) for the glasses studied in this work.

Sample	a	10^3 b	10^{-5} c	st. err[a]
PS DRY	70.0	13.1	-27.9	0.11
PS 0.5	58.9	28.3	-17.1	0.10
PS 1.1	56.5	31.6	-16.3	0.13
PS 2.2	64.1	20.1	-21.9	0.22
PS 3.5	63.5	22.1	-23.0	0.10
AMS DRY	61.4	20.6	-18.1	0.13
AMS-B1 1.3	59.4	23.8	-16.5	0.09
AMS-B1 2.6	49.5	36.1	-9.2	0.07
AMS-B1 3.7	46.1	41.0	-7.3	0.07
AMS-B1 4.8	46.9	42.6	-9.2	0.08
FR DRY	64.6	15.5	-20.5	0.17
FR 1.6	57.7	24.8	-16.0	0.07
FR 2.7	51.6	32.5	-11.3	0.07
FR 3.8	52.6	32.8	-13.3	0.08
FR 6.3	52.1	34.6	-13.3	0.06
ETN DRY	56.5	20.4	-4.7	0.12
ETN 1.4	53.4	23.4	-11.4	0.15
ETN 2.9	51.8	27.3	-13.4	0.08
ETN 3.6	54.8	22.9	-13.0	0.10
ETN 3.8	61.4	13.7	-18.1	0.10

[a] Standar error of estimation

Table 5
Measured and calculated liquid heat capacity for the studied samples.

Sample	Measured Cp ($J\ mol^{-1}\ k^{-1}$)	Calculated[a] Cp ($J\ mol^{-1}\ k^{-1}$)	Δ%*	Calculated[b] Cp ($J\ mol^{-1}\ k^{-1}$)	Δ%*	Calculated[c] Cp ($J\ mol^{-1}\ k^{-1}$)	Δ%*	Calculated[d] Cp ($J\ mol^{-1}\ k^{-1}$)	Δ%*
PS DRY	91.6	93.1	-1.6	90.4	1.3	90.1	1.6	91.6	0.0
PS 0.5	91.5	92.8	-1.5	90.3	1.3	89.8	1.8	90.1	1.5
PS 1.1	91.0	92.7	-1.9	90.2	0.9	89.7	1.4	89.5	1.7
PS 2.2	90.3	92.5	-2.4	90.0	0.4	89.5	0.9	87.8	2.8
PS 3.5	86.1	92.1	-7.0	89.8	-4.2	89.3	-3.7	85.8	0.3
AMS DRY	90.5	97.5	-7.7	94.8	-4.8	93.7	-3.5	90.5	0.0
AMS-B1 1.3	89.6	96.8	-8.0	94.3	-5.2	92.6	-3.3	88.7	1.1
AMS-B1 2.6	86.1	96.3	-11.9	93.9	-9.1	91.9	-6.8	86.3	-0.2
AMS-B1 3.7	84.3	95.9	-13.8	93.6	-11.0	91.5	-8.5	84.5	-0.2
AMS-B1 4.8	83.2	95.5	-14.8	93.3	-12.1	91.2	-9.5	83.0	0.3
FR DRY	94.8	97.4	-2.7	95.2	-0.4	94.4	0.5	94.8	0.0
FR 1.6	93.1	96.7	-3.8	94.6	-1.6	93.3	-0.2	91.8	1.4
FR 2.7	88.1	96.3	-9.3	94.2	-7.0	92.9	-5.5	89.9	-2.1
FR 3.8	85.6	95.8	-12.0	93.9	-9.7	92.5	-8.1	88.1	-3.0
FR 6.3	81.1	95.0	-17.1	93.2	-14.9	91.9	-13.3	84.2	-3.8
ETN DRY	96.6	98.6	-2.1	97.5	-0.9	95.7	0.9	96.6	0.0
ETN 1.4	95.6	97.9	-2.5	96.9	-1.3	95.1	0.5	93.7	2.0
ETN 2.9	91.1	97.3	-6.8	96.3	-5.6	94.6	-3.8	91.1	0.0
ETN 3.6	90.4	97.0	-7.3	96.0	-6.2	94.5	-4.5	89.9	0.6
ETN 3.8	89.5	96.9	-8.4	95.9	-7.3	94.4	-5.5	89.7	-0.3

[a] Calculated values using the Lange and Navrotsky (1992) model

[b] Calculated values using the Stebbins et al. (1984) model

[c] Calculated values using the Richet and Bottinga (1985) model with Cp of Al_2O_3 reported by Courtial and Richet (1993)

[c] Calculated values using Eq. 2 and Eq. 3

100 (Measured Cp − Calculated Cp)/Measured Cp

Table 6
Measured and calculated liquid heat capacity for the studied samples using a partial molar heat capacity for water in depolymerized melts of 237 J/mol K reported in Bouhinfd et al., 2012.

Sample	Measured Cp ($J\ mol^{-1}\ k^{-1}$)	Calculated[a] Cp ($J\ mol^{-1}\ k^{-1}$)	Δ%*	Calculated[b] Cp ($J\ mol^{-1}\ k^{-1}$)	Δ%*	Calculated[c] Cp ($J\ mol^{-1}\ k^{-1}$)	Δ%*
FR 1.6	93.1	105.3	-13.1	103.2	-10.8	101.9	-9.4
FR 2.7	88.1	110.2	-25.2	108.2	-22.9	106.8	-21.3
FR 3.8	85.6	114.8	-34.1	112.8	-31.8	111.4	-30.2
FR 6.3	81.1	124.0	-52.9	122.2	-50.7	120.9	-49.0
ETN 1.4	95.6	105.4	-10.3	104.3	-9.2	102.6	-7.3
ETN 2.9	91.1	112.0	-22.9	110.9	-21.7	109.3	-19.9
ETN 3.6	90.4	114.8	-27.0	113.8	-25.9	112.3	-24.2
ETN 3.8	89.5	115.6	-29.2	114.6	-28.1	113.1	-26.4

[a] Calculated values using the Lange and Navrotsky (1992) model

[b] Calculated values using the Stebbins et al. (1984) model

[c] Calculated values using the Richet and Bottinga (1985) model with Cp of Al_2O_3 reported by Courtial and Richet (1993)

[d] 100* (Measured Cp − Calculated Cp)/Measured Cp

Table 7

Calculated partial molar heat capacity of molecular water ($Cp_{H2Omol.}$) and OH^- (Cp_{OH-}) using Eq. 4.

	NBO/T[a]	$Cp_{H2Omol.}$	Cp_{OH-}	Err.[b]	SM[c]
AMS-B1	0.10	18.87	80.33	0.56	20.51
PS	0.11	0.00	144.73	0.39	16.02
ETN	0.45	21.29	68.22	0.74	32.39

[a]NBO/T = (Mysen, 1988).

[b]Average relative error.

[c] Sum of structure modifying oxides (Giordano and Dingwell, 2003).

Table 8

Fit parameters of FR (Misiti et al., 2011) and AMS-B1 (Romano et al.,2001 and Misiti et al., 2006) according to Eq. (8). Numbers in parenthesis are standard

Parameters	**FR**		**AMS-B1**	
A_{VFT}	-4.55		-4.55	
b_1	7631.61	(±236.88)	11495.04	(±277.84)
b_2	-2041.55	(±766.30)	-5528.46	(±549.27)
c_1	488.45	(±18.90)	202.47	(±21.20)
c_2	-305.85	(±81.89)	-27.57	(±4.18)
St. Err.	0.51		0.29	

Table 9

Calculated steepness index *m* (e.g., Plazek and Ngai, 1991) for AMS-B1and FR sample as a function of water content.

Sample	H_2O (mol%)	*m*
AMS-B1 DRY	-	21.4
AMS-B1 1.3	4.66	22.1
AMS-B1 2.6	8.97	22.6
AMS-B1 3.7	12.46	23.0
AMS-B1 4.8	15.79	23.4
FR DRY	-	34.1
FR 1.6	5.61	31.2
FR 2.7	9.22	29.9
FR 3.8	12.55	28.9
FR 6.3	19.86	27.0